Supporting Information

for

Syntheses and reactivity of the apically functionalized (pseudo)macrobicyclic iron(II) tris-dioximates and their hybrid phthalocyaninatoclathrochelate derivatives comprising reactive and vector terminal group

Alexander S. Chuprin[a], Semyon V. Dudkin[a], Svetlana A. Belova[a,b], Ekaterina G. Lebed[a,b], Pavel V. Dorovatovskii,[c] Anna V. Vologzhanina[a], Yan Z. Voloshin[a,b]

[a] *Nesmeyanov Institute of Organoelement Compounds of the Russian Academy of Sciences, 28 Vavilova st., 119991 Moscow, Russia*

[b] *Kurnakov Institute of General and Inorganic Chemistry of the Russian Academy of Sciences, 31 Leninsky pr., 119991 Moscow, Russia*

[c] *National Research Center "Kurchatov Institute", 1 Acad. Kurchatov Sq., 123182 Moscow, Russian Federation*

@*Corresponding author E-mail:* voloshin@ineos.ac.ru

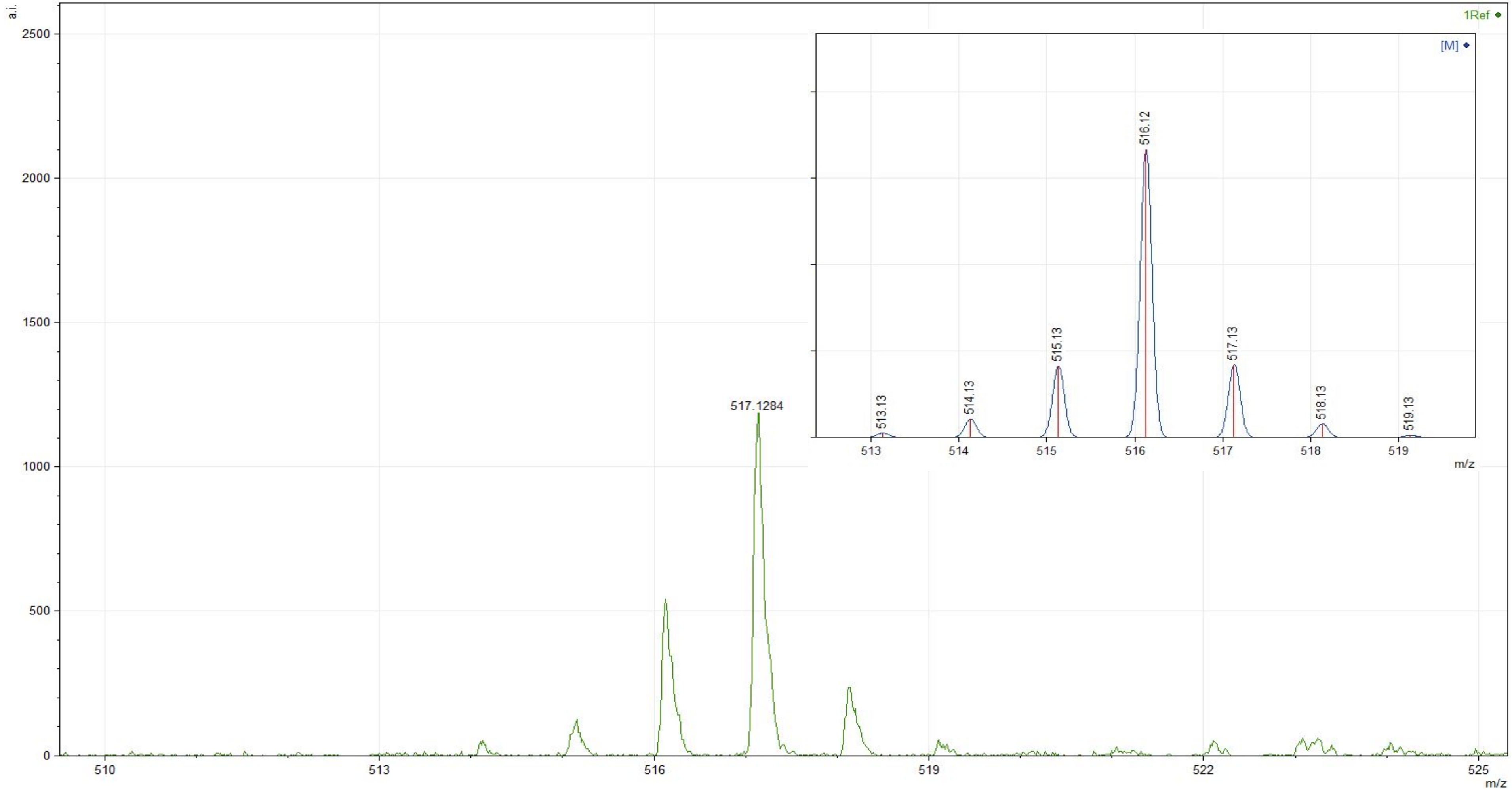

Fig. S1. Fragment of the MALDI-TOF mass spectrum of the semiclathrochelate FeDm(HDm)$_2$(B4-C$_6$H$_4$CHO) in its positive range. Insert: the theoretically calculated isotopic distribution in its molecular ion.

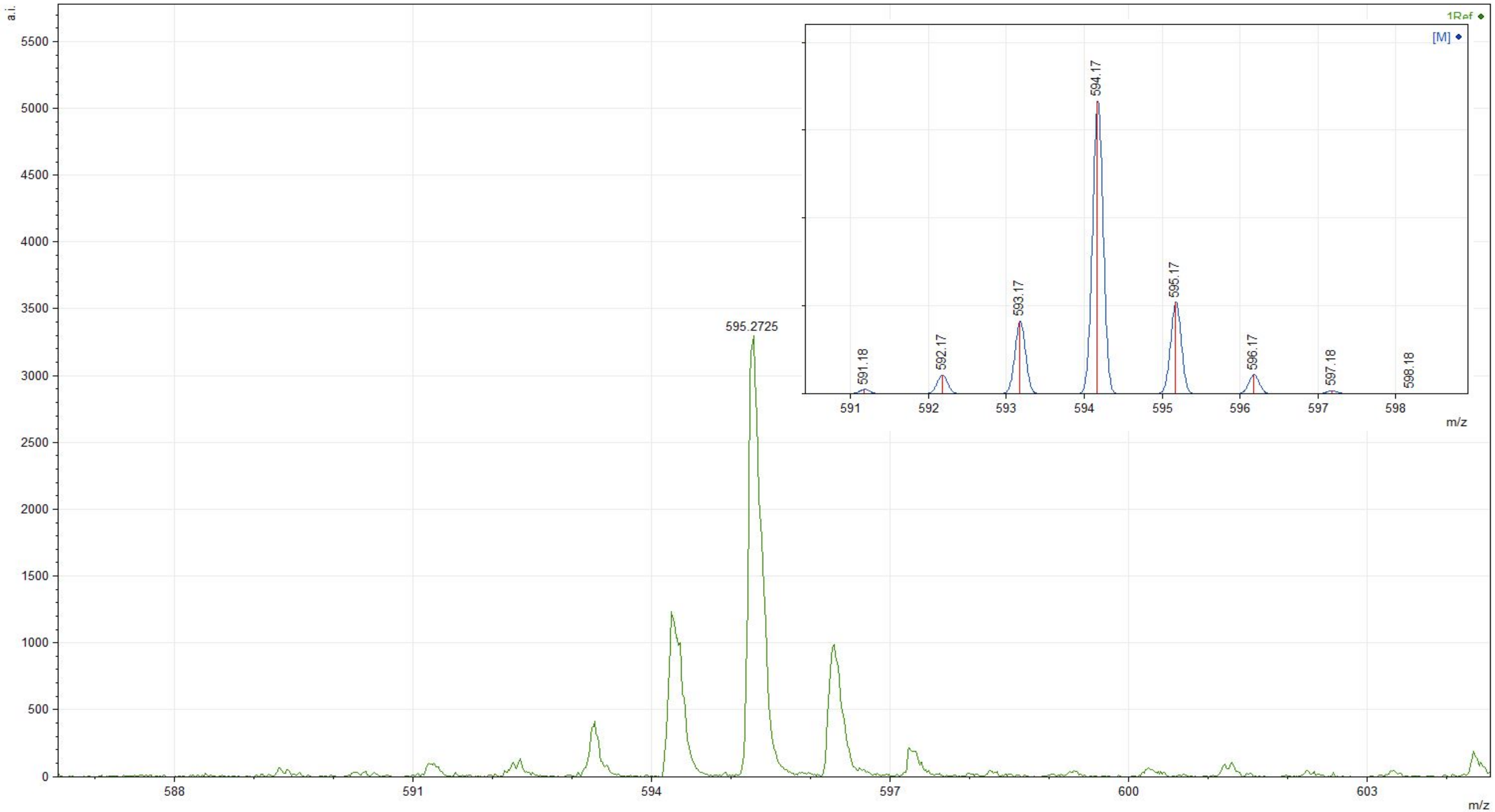

Fig. S2. Fragment of the MALDI-TOF mass spectrum of the semiclathrochelate FeNx(HNx)$_2$(B4-C$_6$H$_4$CHO) in its positive range. Insert: the theoretically calculated isotopic distribution in its molecular ion.

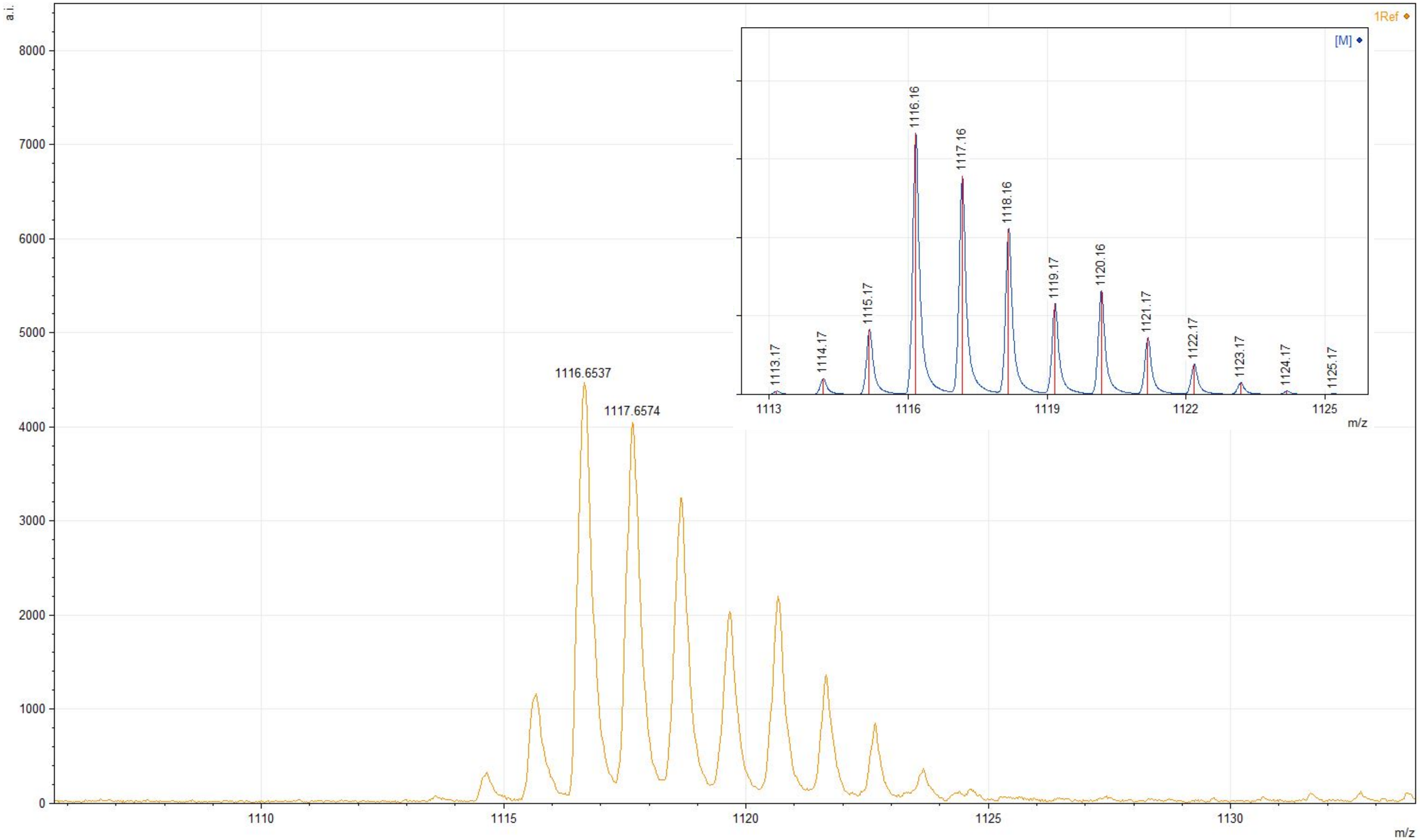

Fig. S3. Fragment of the MALDI-TOF mass spectrum of the phthalocyaninatoclathrochelate $FeDm_3(B4\text{-}C_6H_4CHO)(ZrPc)$ in its positive range. Insert: the theoretically calculated isotopic distribution in its molecular ion.

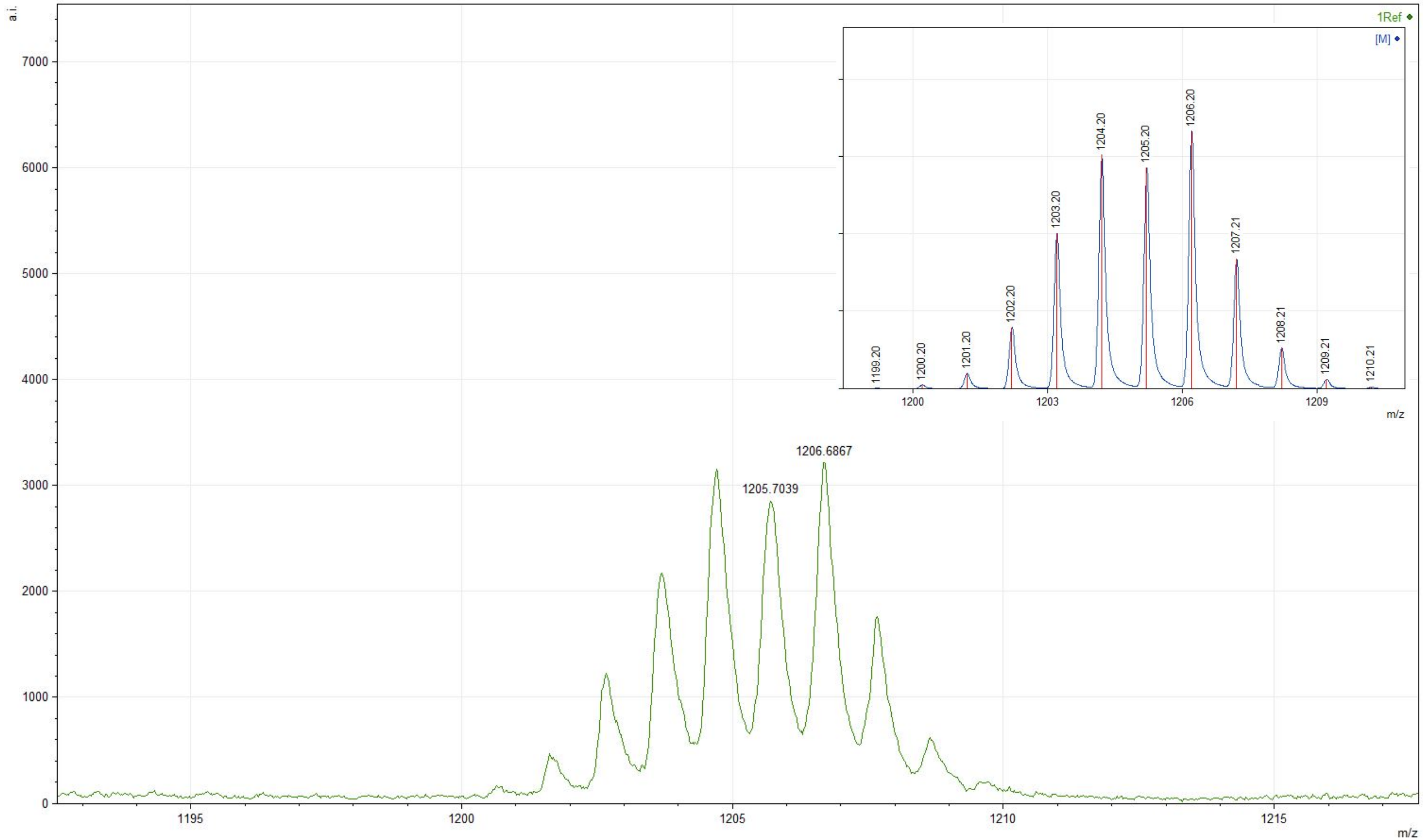

Fig. S4. Fragment of the MALDI-TOF mass spectrum of the phthalocyaninatoclathrochelate $FeDm_3(B4\text{-}C_6H_4CHO)(HfPc)$ in its positive range. Insert: the theoretically calculated isotopic distribution in its molecular ion.

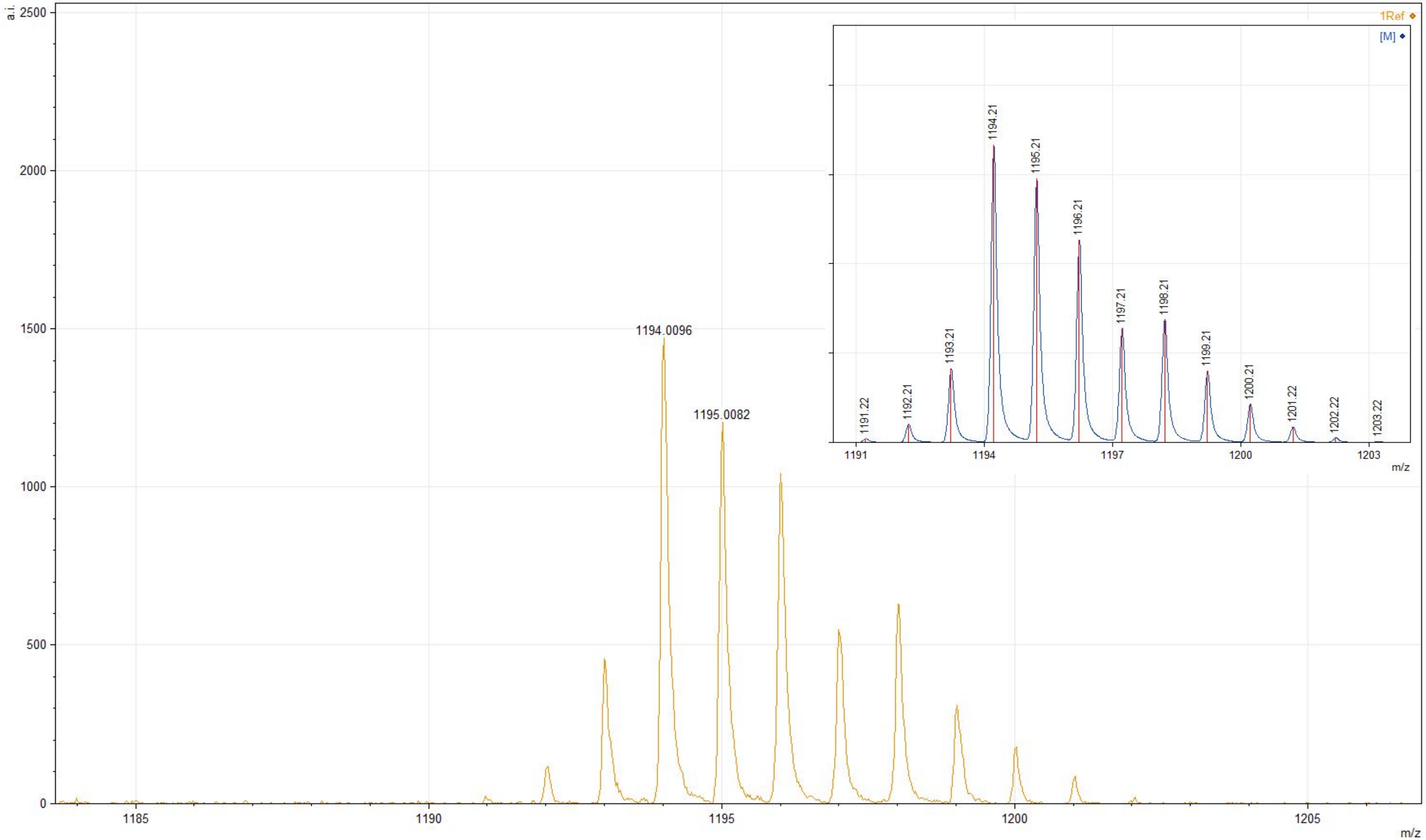

Fig. S5. Fragment of the MALDI-TOF mass spectrum of the phthalocyaninatoclathrochelate $FeNx_3(B4\text{-}C_6H_4CHO)(ZrPc)$ in its positive range. Insert: the theoretically calculated isotopic distribution in its molecular ion.

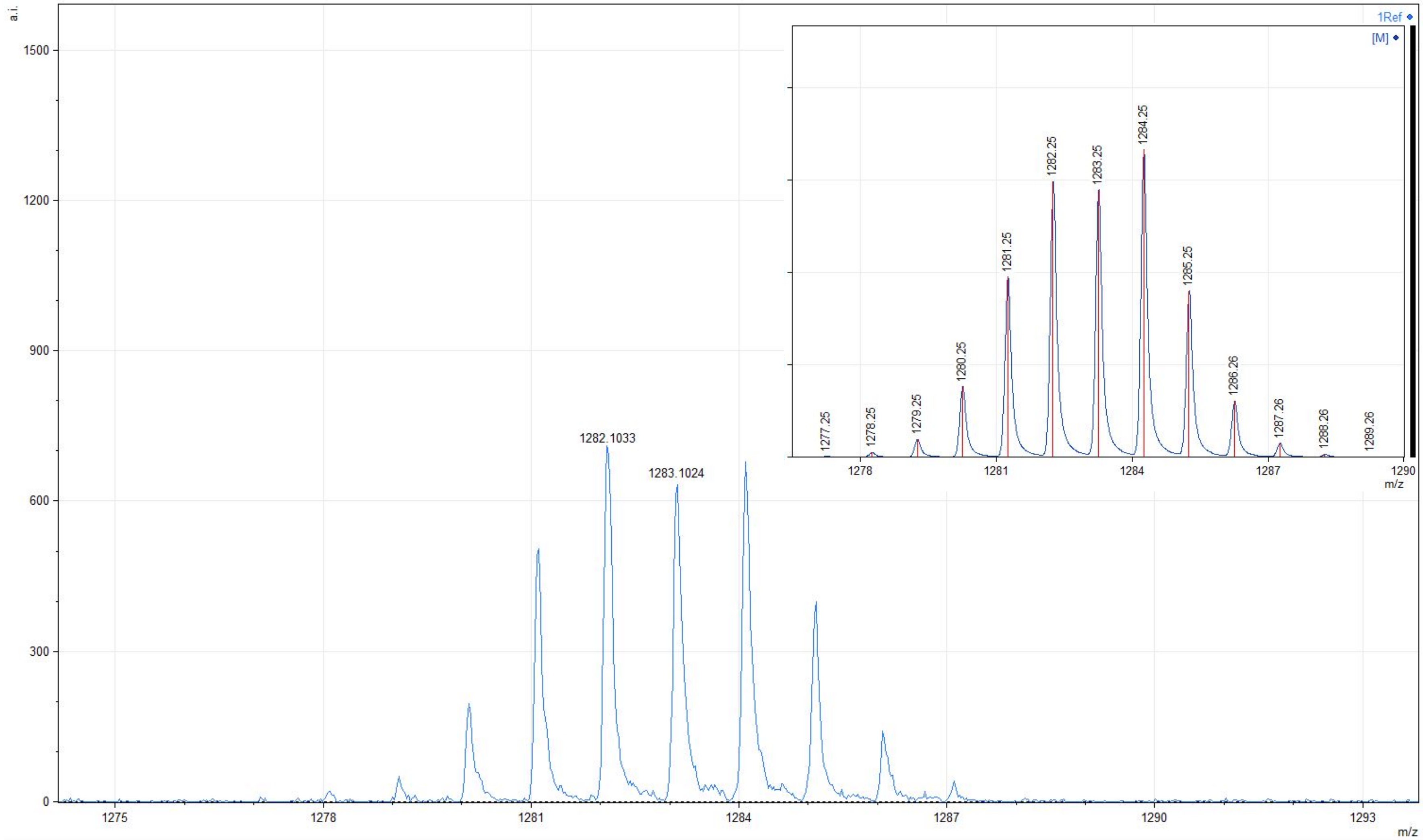

Fig. S6. Fragment of the MALDI-TOF mass spectrum of the phthalocyaninatoclathrochelate $FeNx_3(B4\text{-}C_6H_4CHO)(HfPc)$ in its positive range. Insert: the theoretically calculated isotopic distribution in its molecular ion.

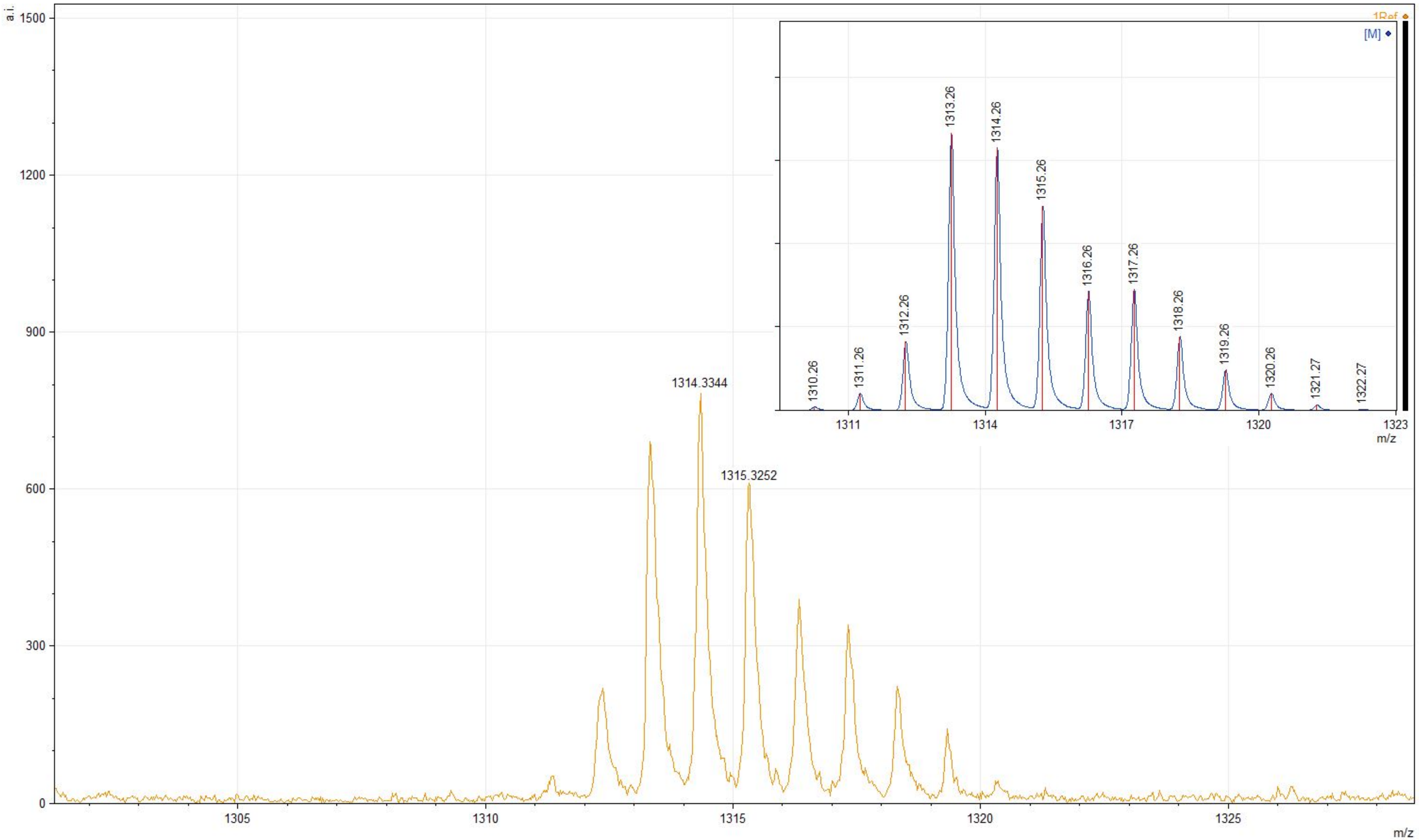

Fig. S7. Fragment of the MALDI-TOF mass spectrum of the hybrid phthalocyaninatoclathrochelate $FeNx_3(B4\text{-}C_6H_4Id)(ZrPc)$ in its positive range. Insert: the theoretically calculated isotopic distribution in its molecular ion.

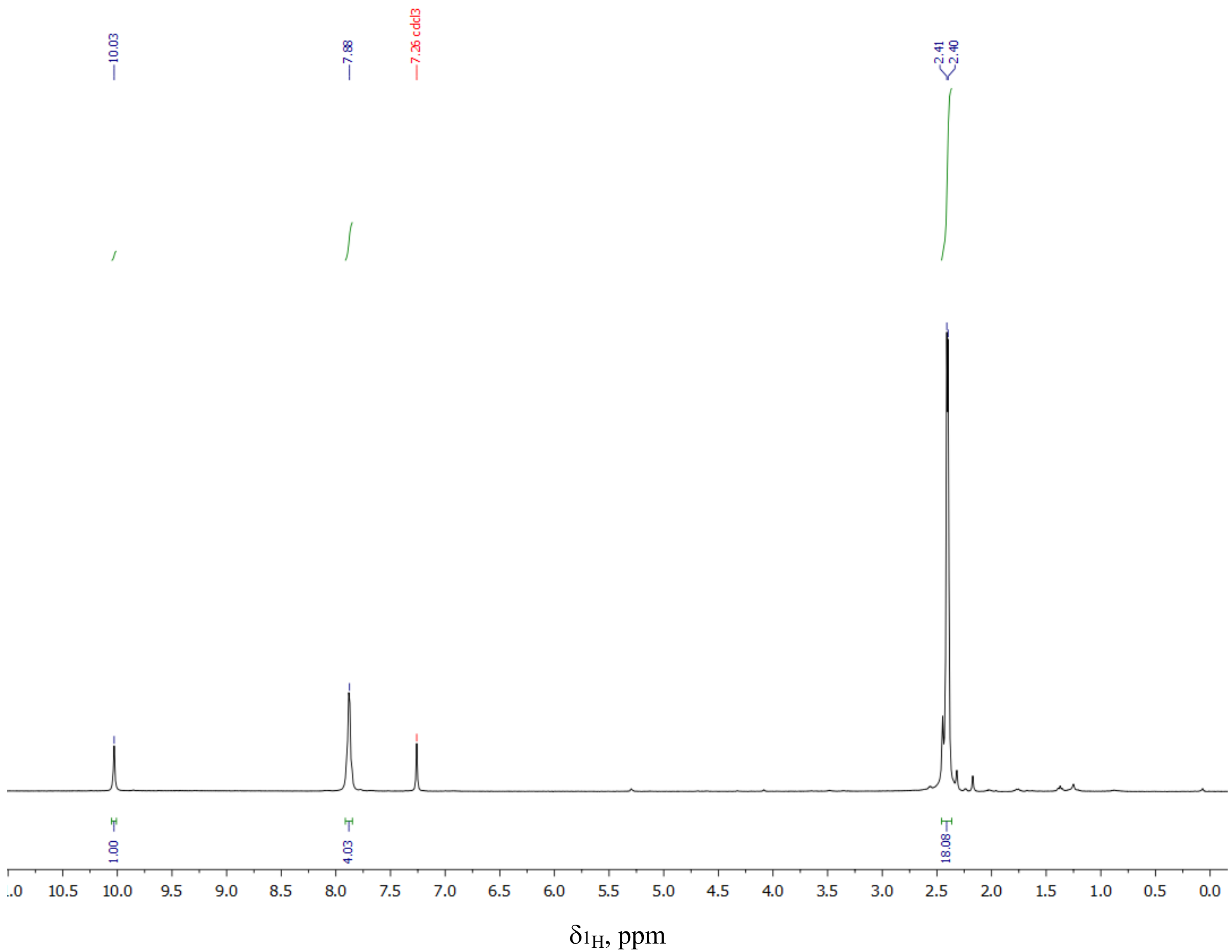

Fig. S8. ^{1}H NMR spectrum of the semiclathrochelate FeDm(HDm)$_2$(B4-C$_6$H$_4$CHO) in CDCl$_3$.

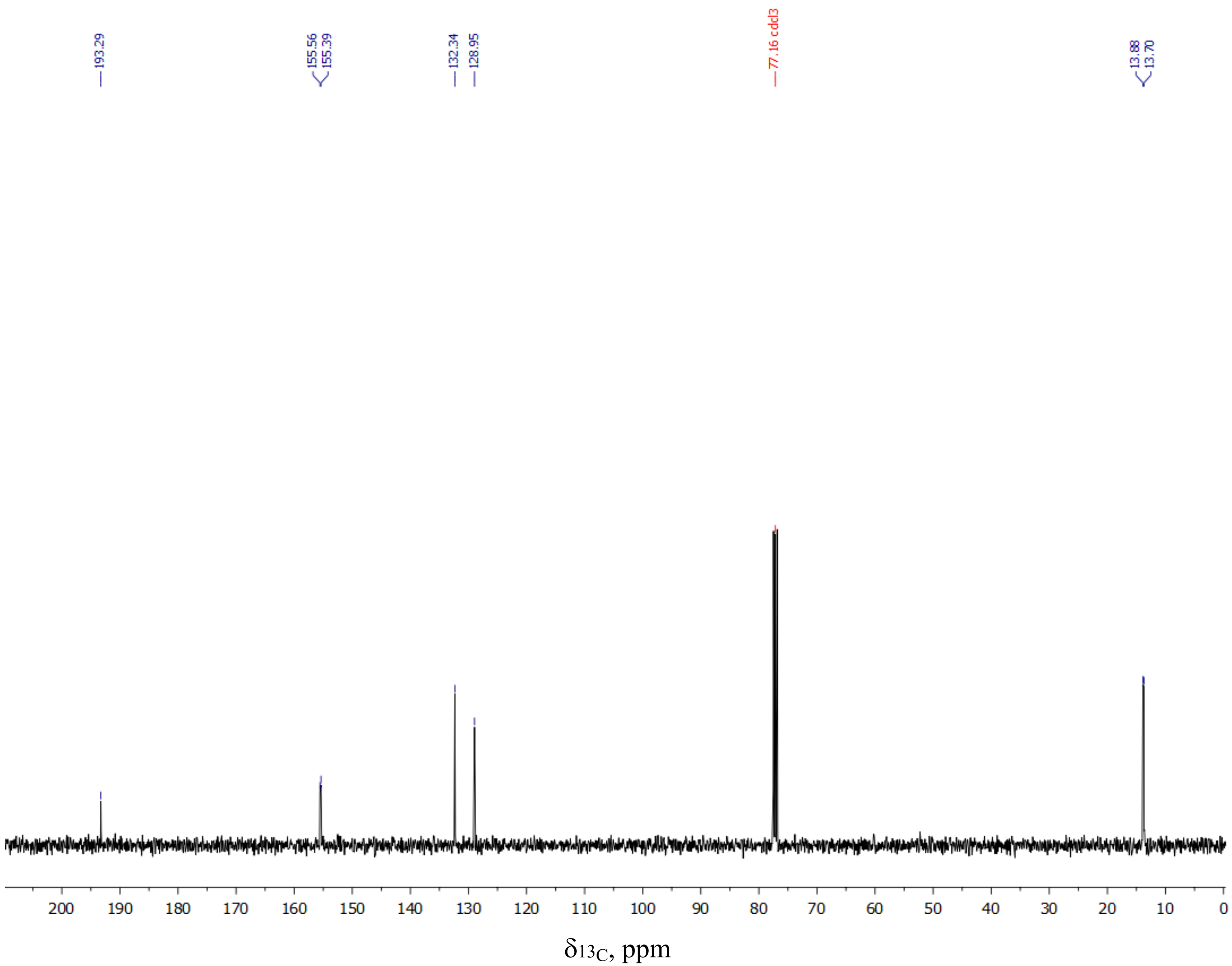

Fig. S9. $^{13}C\{^1H\}$ NMR spectrum of the semiclathrochelate $FeDm(HDm)_2(B4\text{-}C_6H_4CHO)$ in $CDCl_3$.

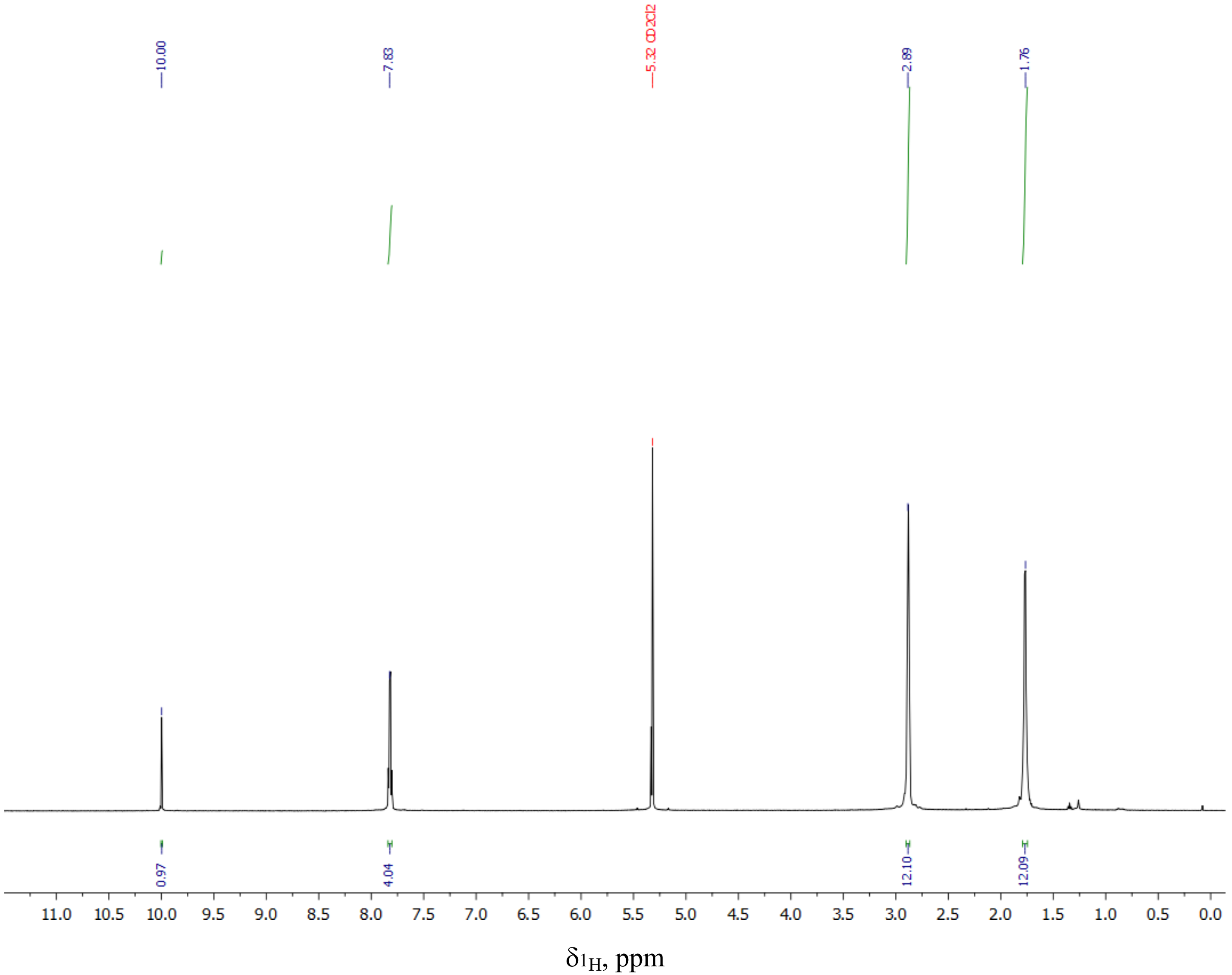

Fig. S10. ^{1}H NMR spectrum of the semiclathrochelate $FeNx(HNx)_2(B4\text{-}C_6H_4CHO)$ in CD_2Cl_2.

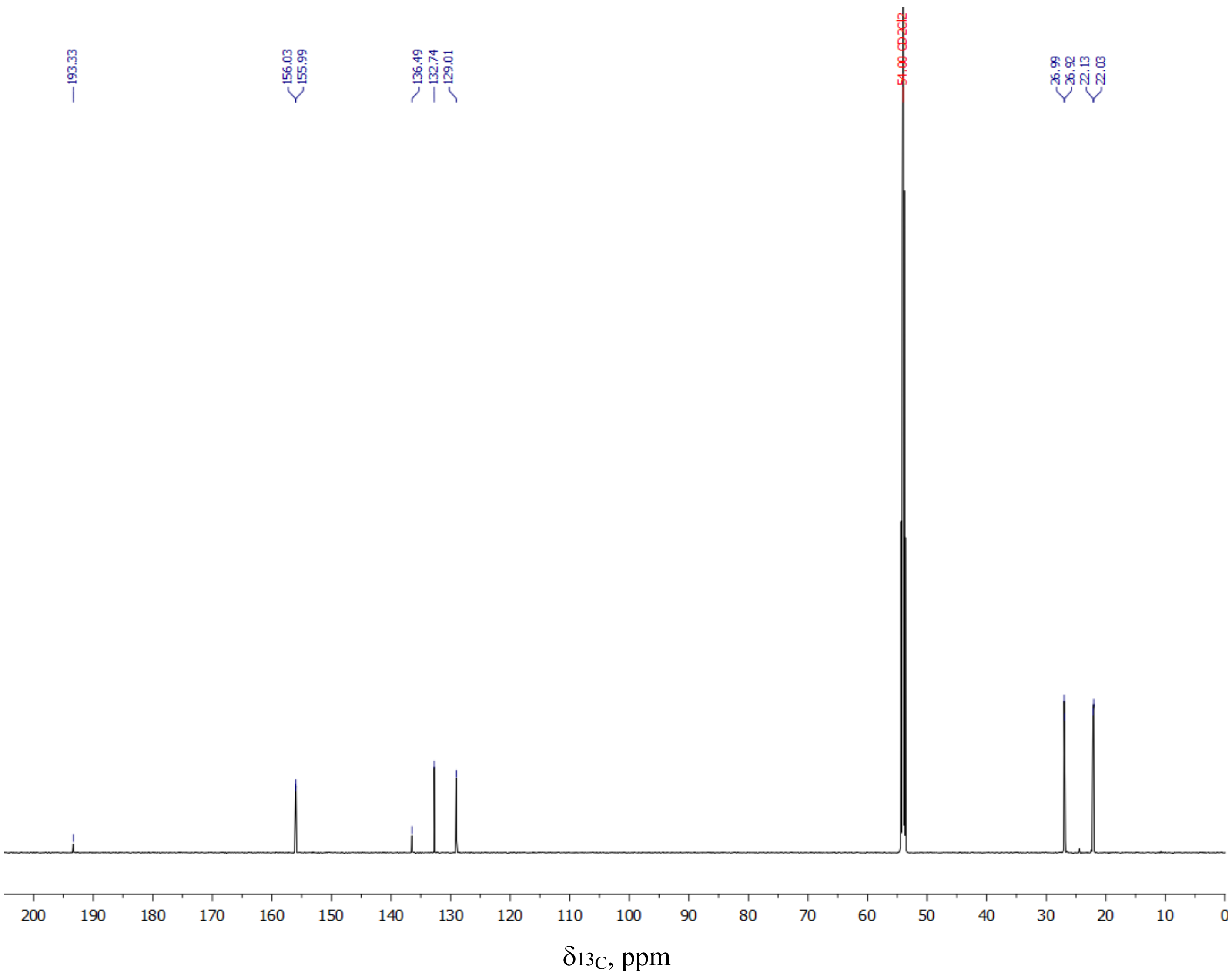

Fig. S11. $^{13}C\{^{1}H\}$ NMR spectrum of the semiclathrochelate $FeNx(HNx)_2(B4\text{-}C_6H_4CHO)$ in CD_2Cl_2.

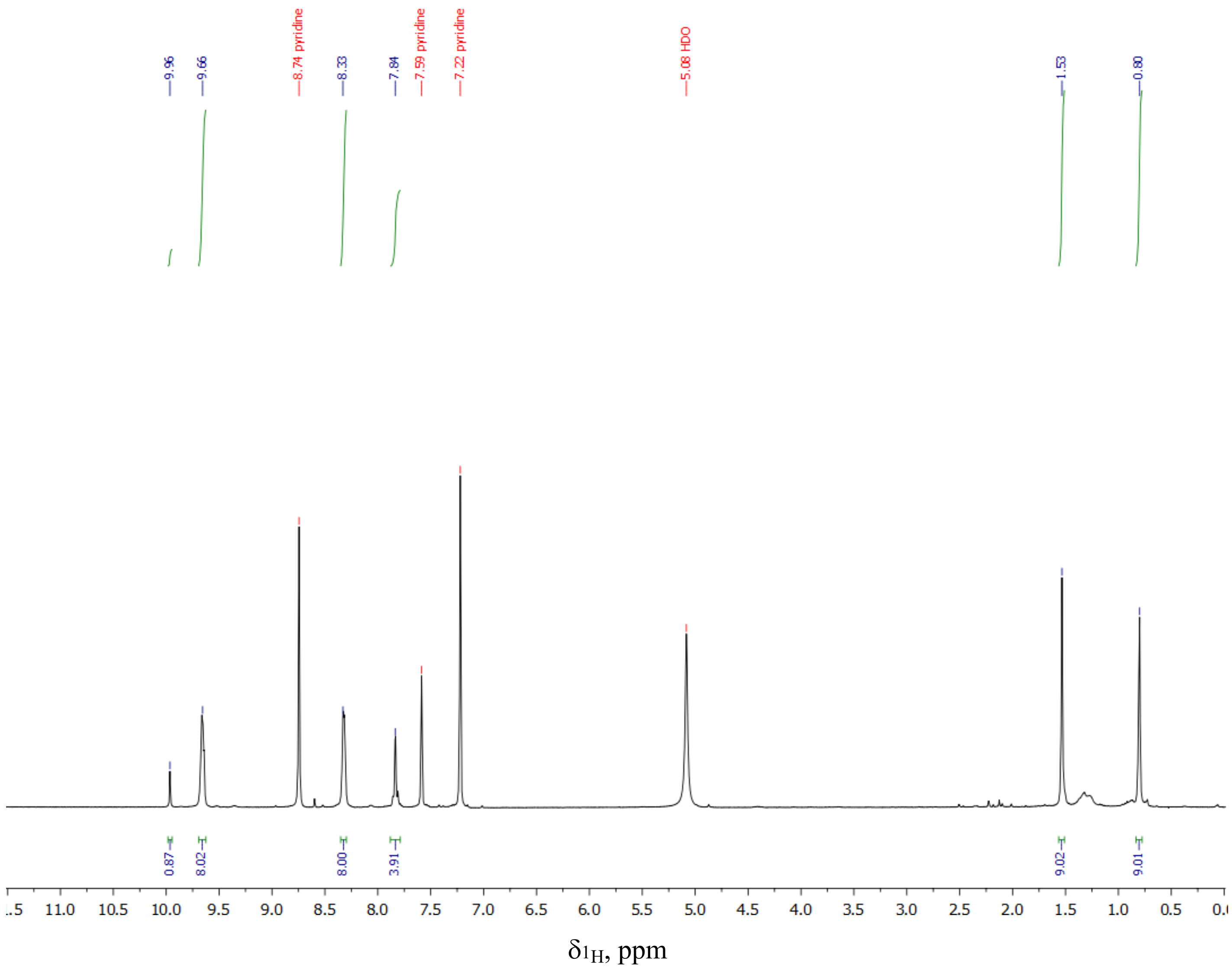

Fig. S12. [1]H NMR spectrum of the phthalocyaninatoclathrochelate $FeDm_3(B4-C_6H_4CHO)(ZrPc)$ in pyridine-d_5.

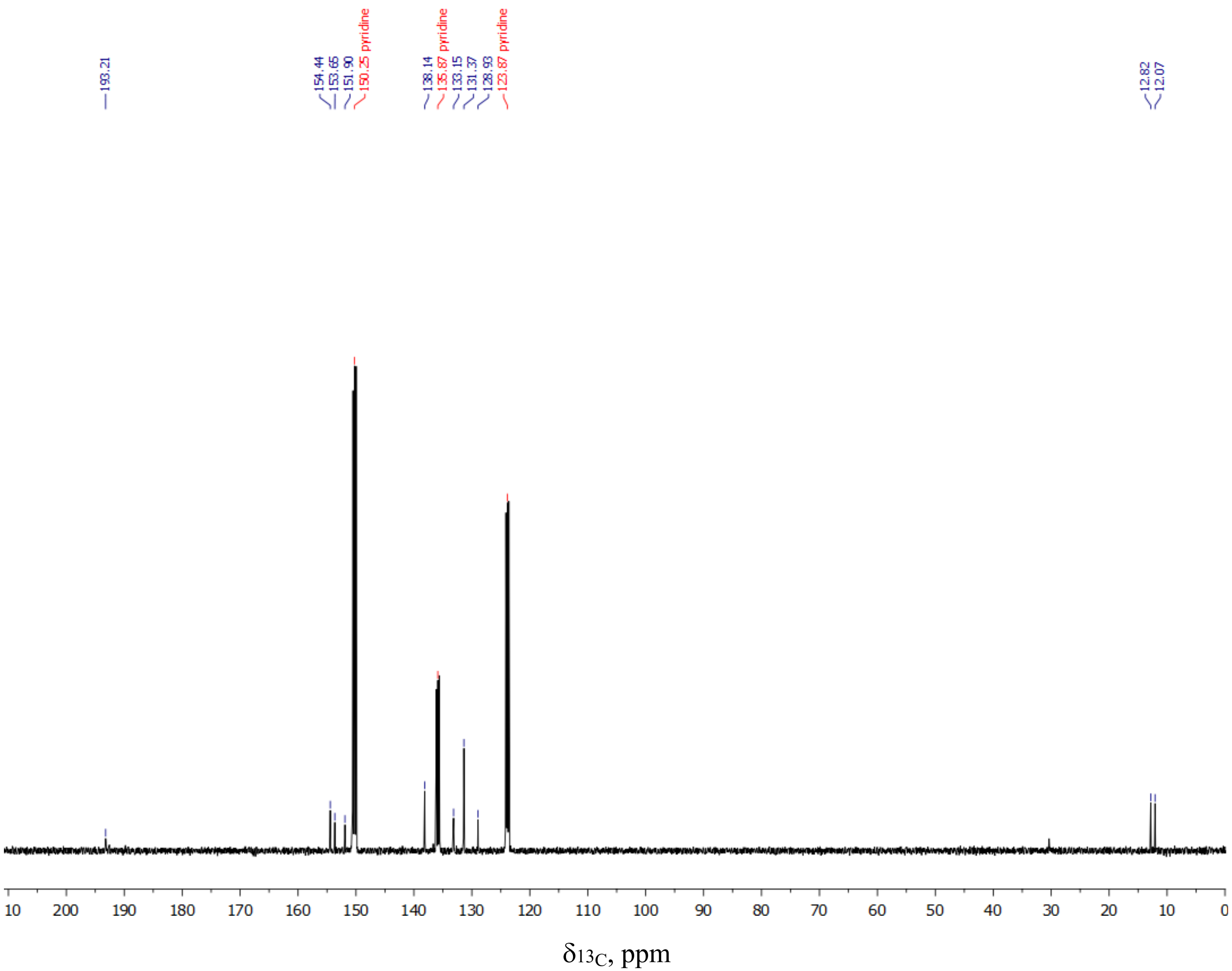

Fig. S13. $^{13}C\{^1H\}$ NMR spectrum of the phthalocyaninatoclathrochelate $FeDm_3(B4\text{-}C_6H_4CHO)(ZrPc)$ in pyridine-d_5.

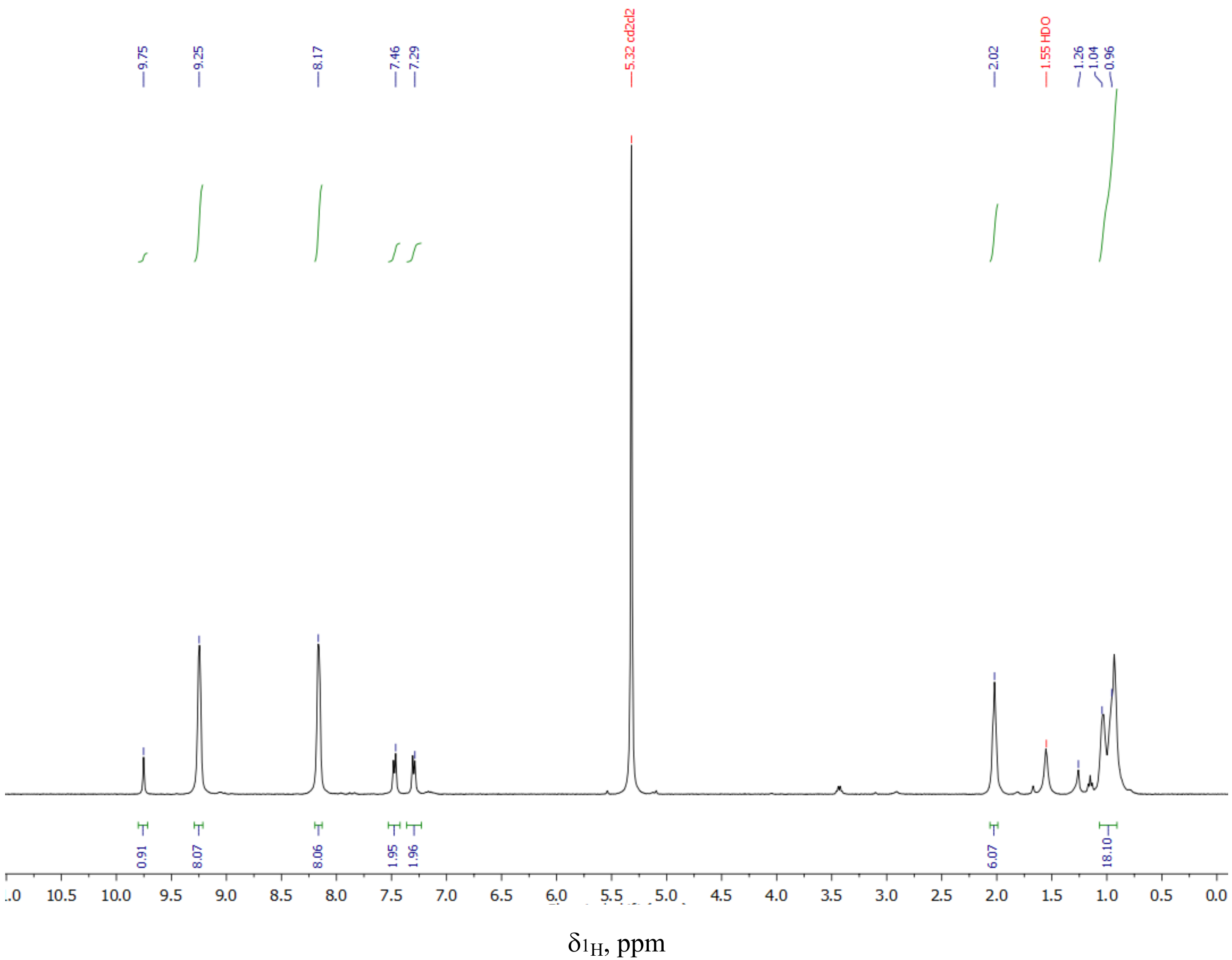

Fig. S14. ¹H NMR spectrum of the phthalocyaninatoclathrochelate $FeNx_3(B4\text{-}C_6H_4CHO)(ZrPc)$ in CD_2Cl_2.

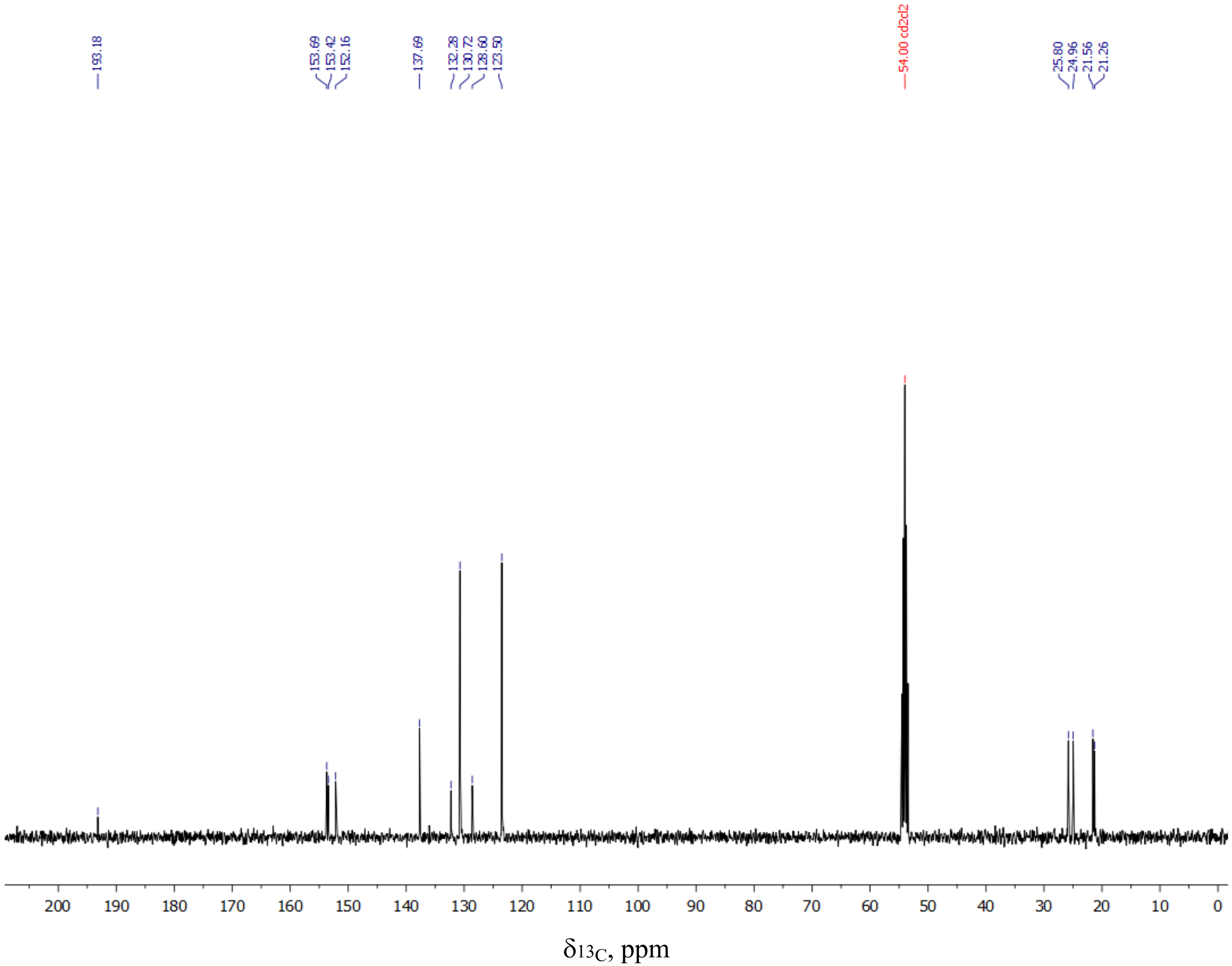

Fig. S15. $^{13}C\{^{1}H\}$ NMR spectrum of the phthalocyaninatoclathrochelate $FeNx_3(B4\text{-}C_6H_4CHO)(ZrPc)$ in CD_2Cl_2.

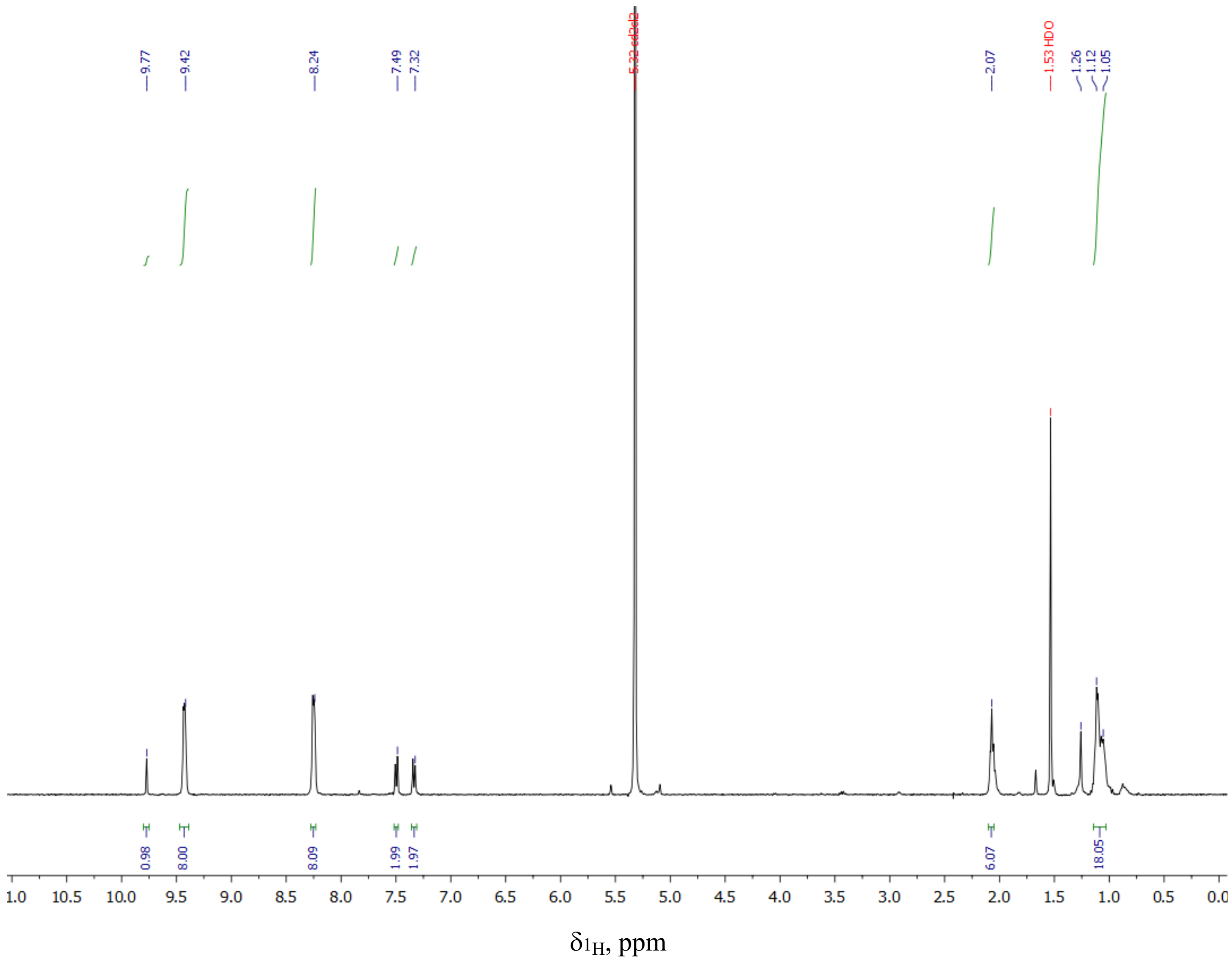

Fig. S16. ^{1}H NMR spectrum of the phthalocyaninatoclathrochelate $FeNx_3(B4\text{-}C_6H_4CHO)(HfPc)$ in CD_2Cl_2.

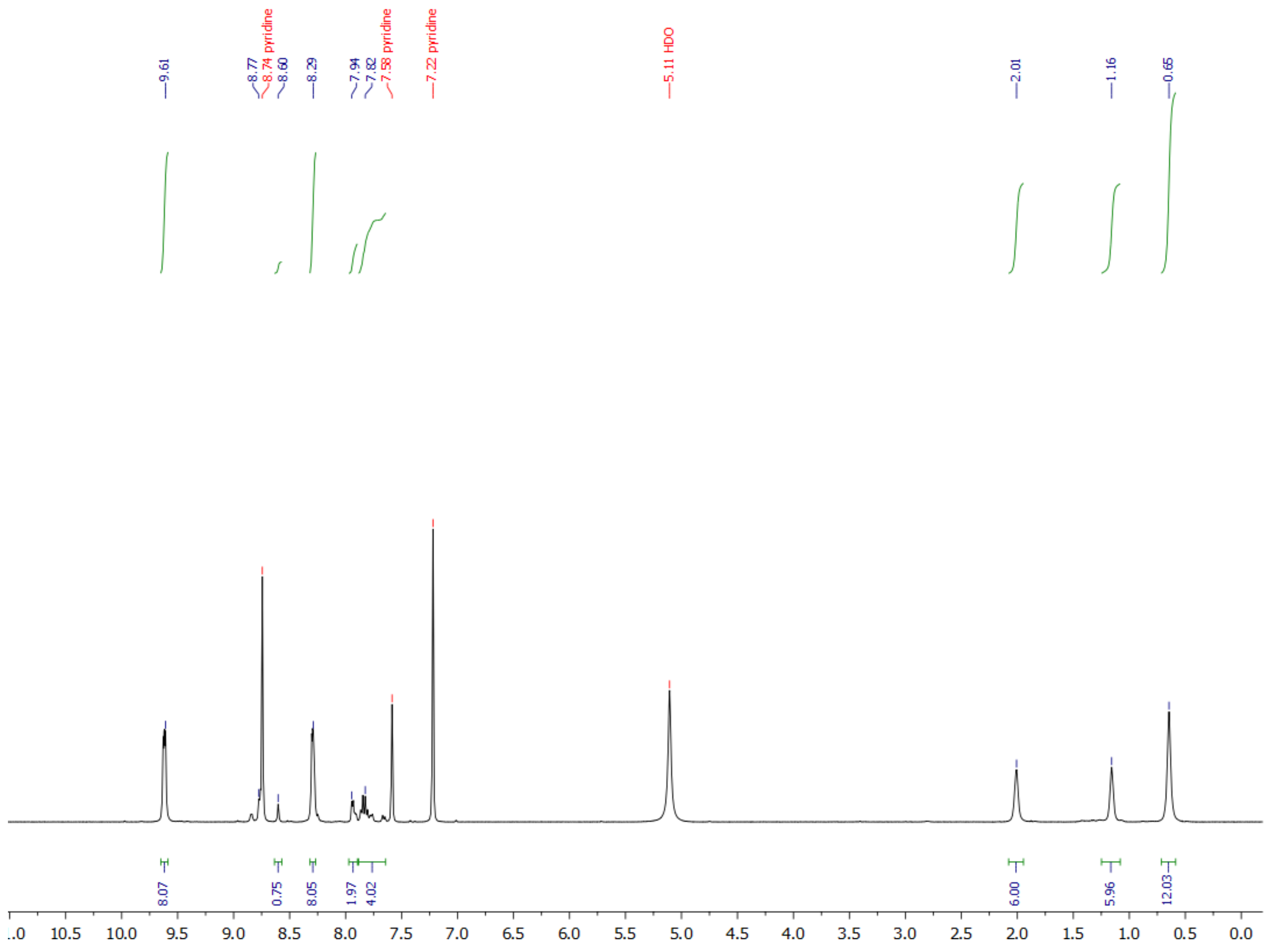

Fig. S17. ^{1}H NMR spectrum of the hybrid phthalocyaninatoclathrochelate $FeNx_3(B4\text{-}C_6H_4Id)(ZrPc)$ in pyridine-*d*$_5$.

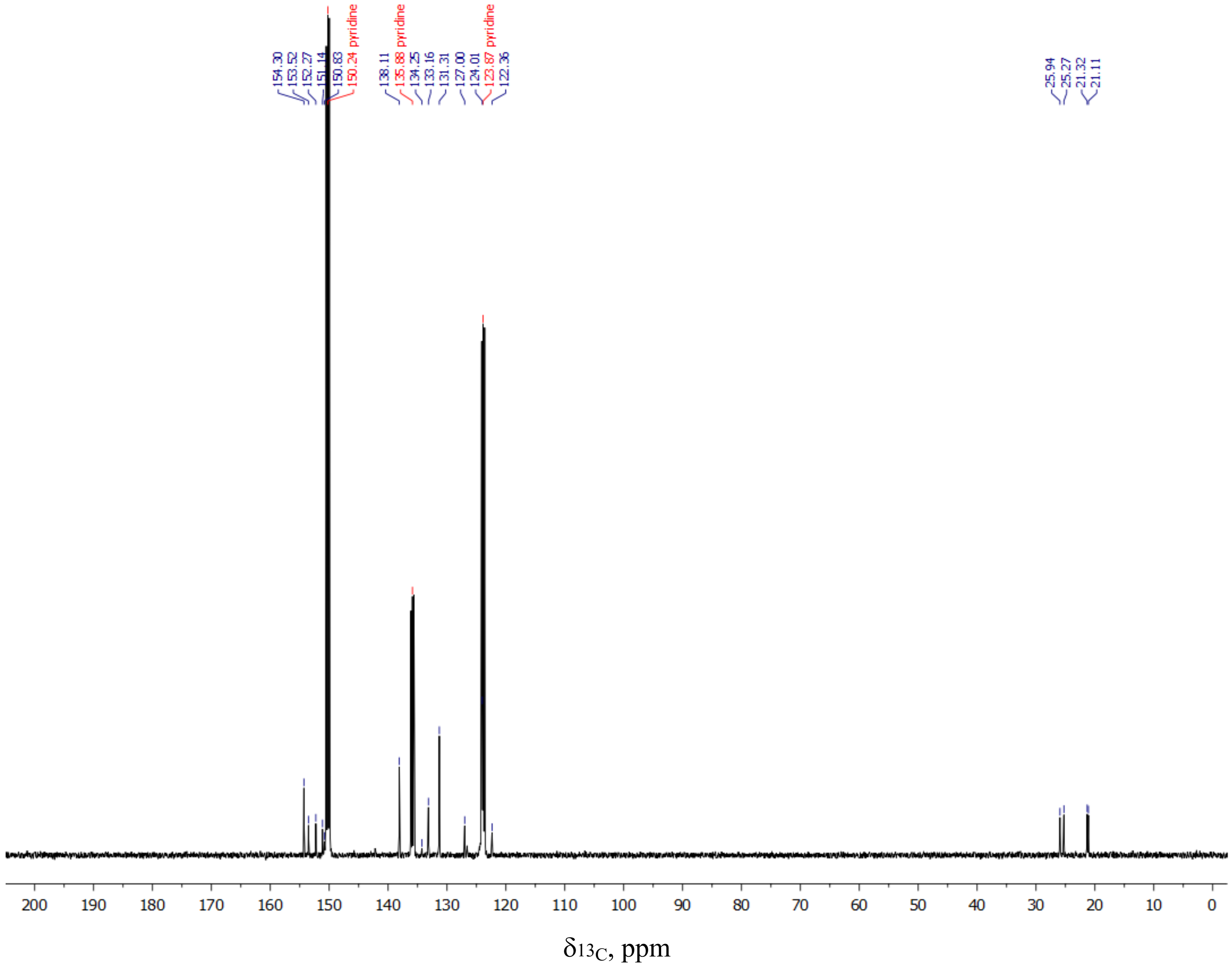

Fig. S18. $^{13}C\{^1H\}$ NMR spectrum of the hybrid phthalocyaninatoclathrochelate $FeNx_3(B4\text{-}C_6H_4Id)(ZrPc)$ in pyridine-d_5.

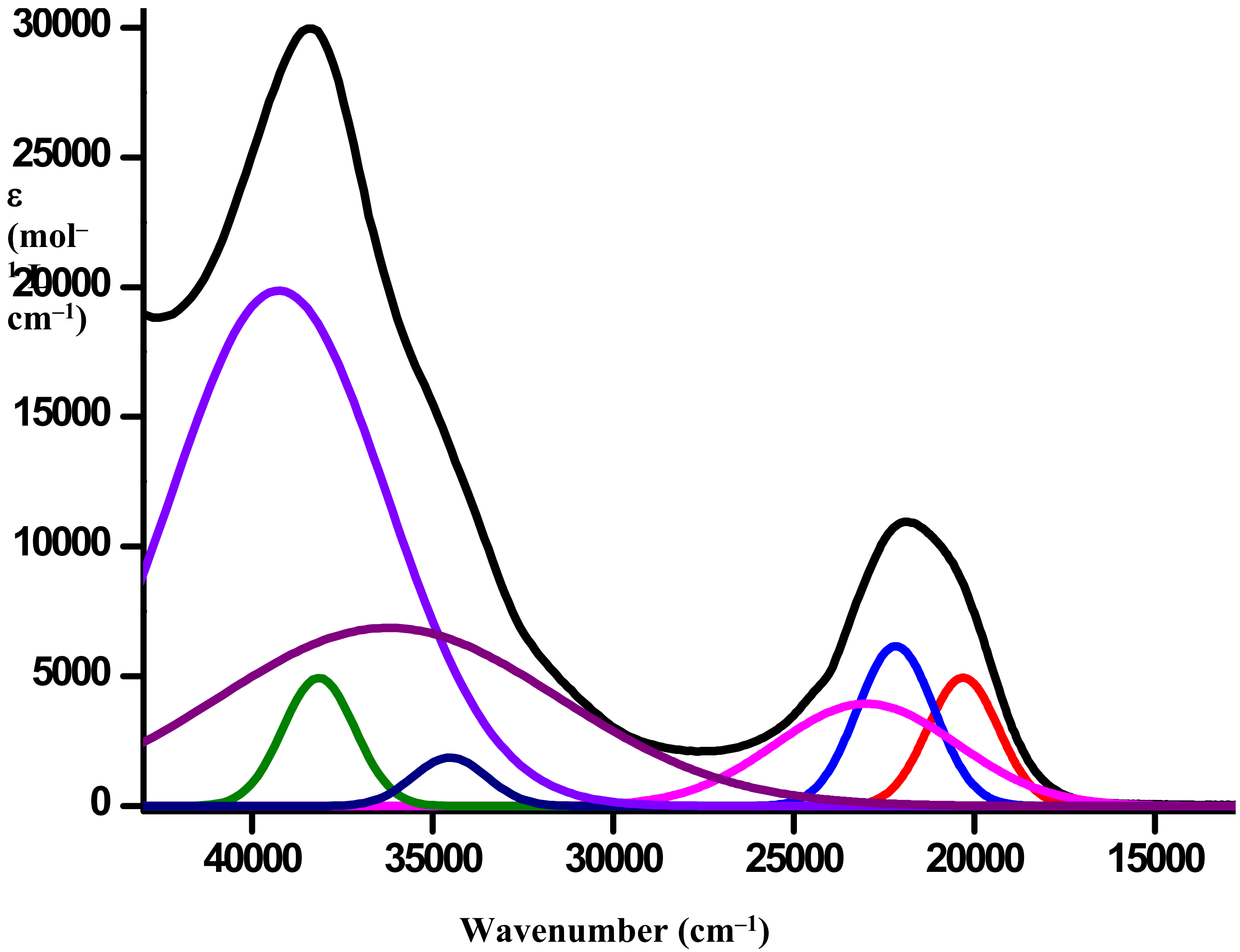

Fig. S19. Solution UV-vis spectrum of the semiclathrochelate FeDm(HDm$_2$)(B4-C_6H_4CHO)in CH_2Cl_2 (shown in black line) and its deconvolution into the Gaussian components (shown in color lines).

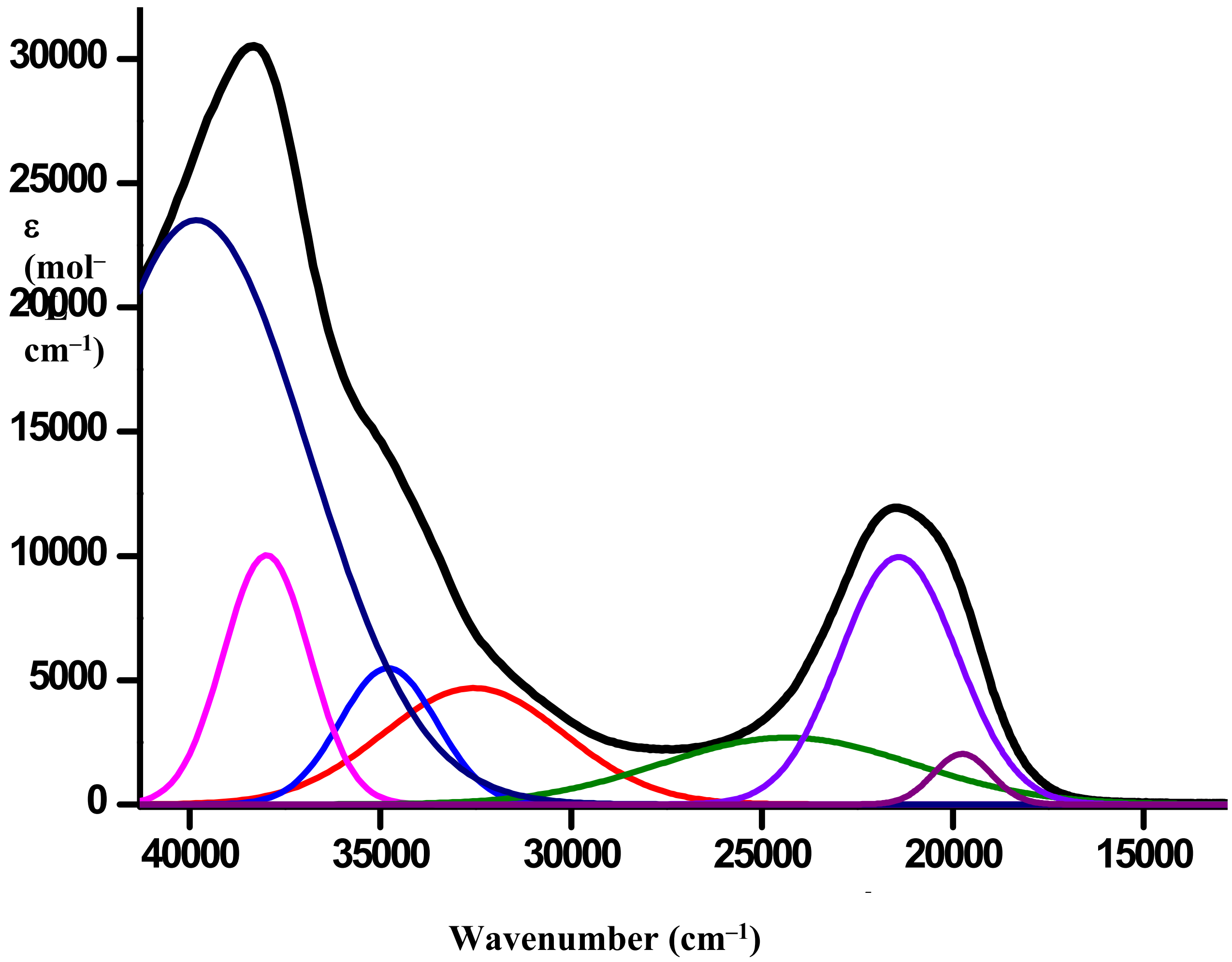

Fig. S20. Solution UV-vis spectrum of the semiclathrochelate FeNx(HNx$_2$)(B4-C_6H_4CHO) in CH_2Cl_2 (shown in black line) and its deconvolution into the Gaussian components (shown in color lines).

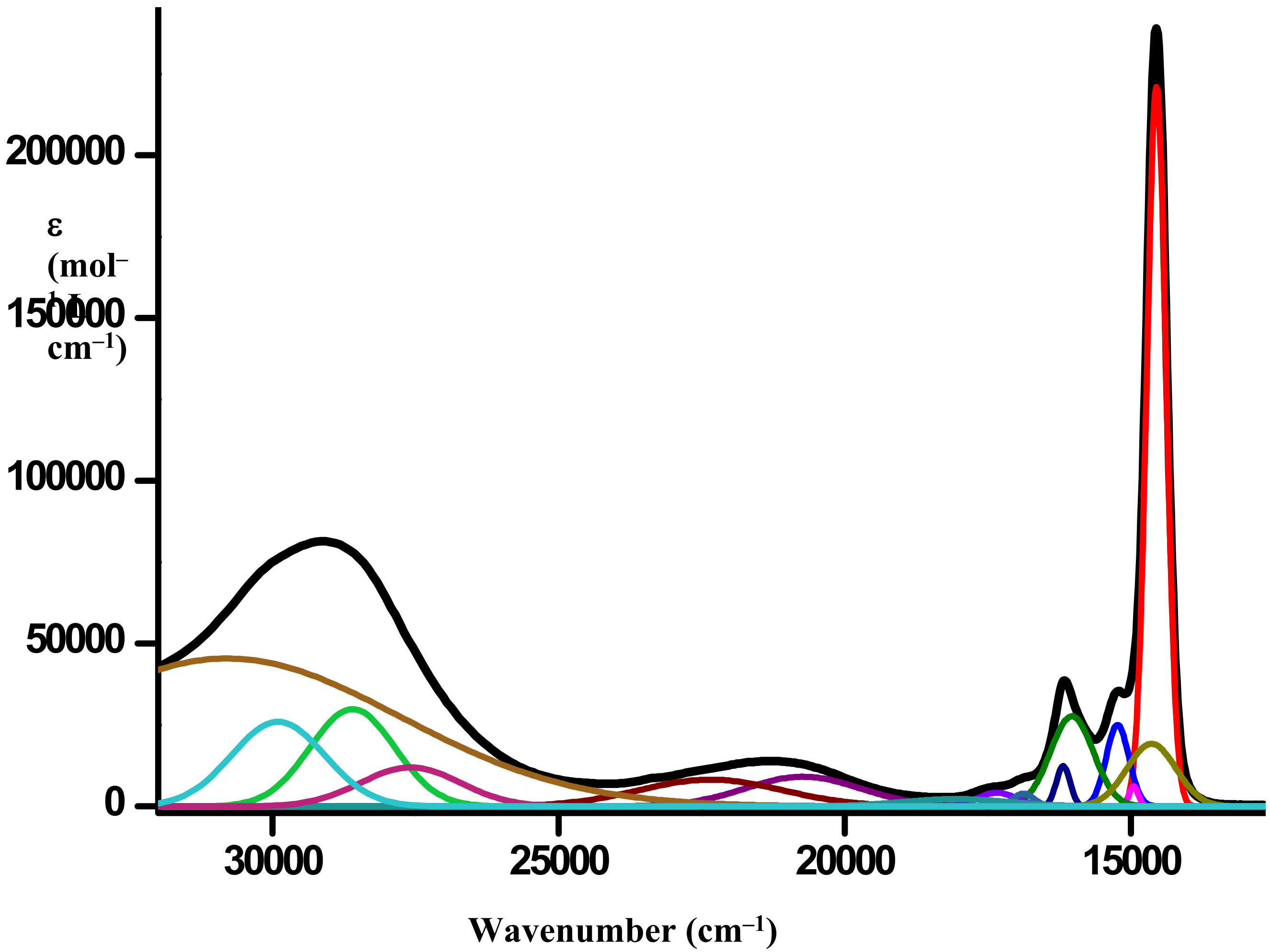

Fig. S21. Solution UV-vis spectrum of the phthalocyaninatoclathrochelate $FeDm_3(B4\text{-}C_6H_4CHO)(ZrPc)$ in CH_2Cl_2 (shown in black line) and its deconvolution into the Gaussian components (shown in color lines).

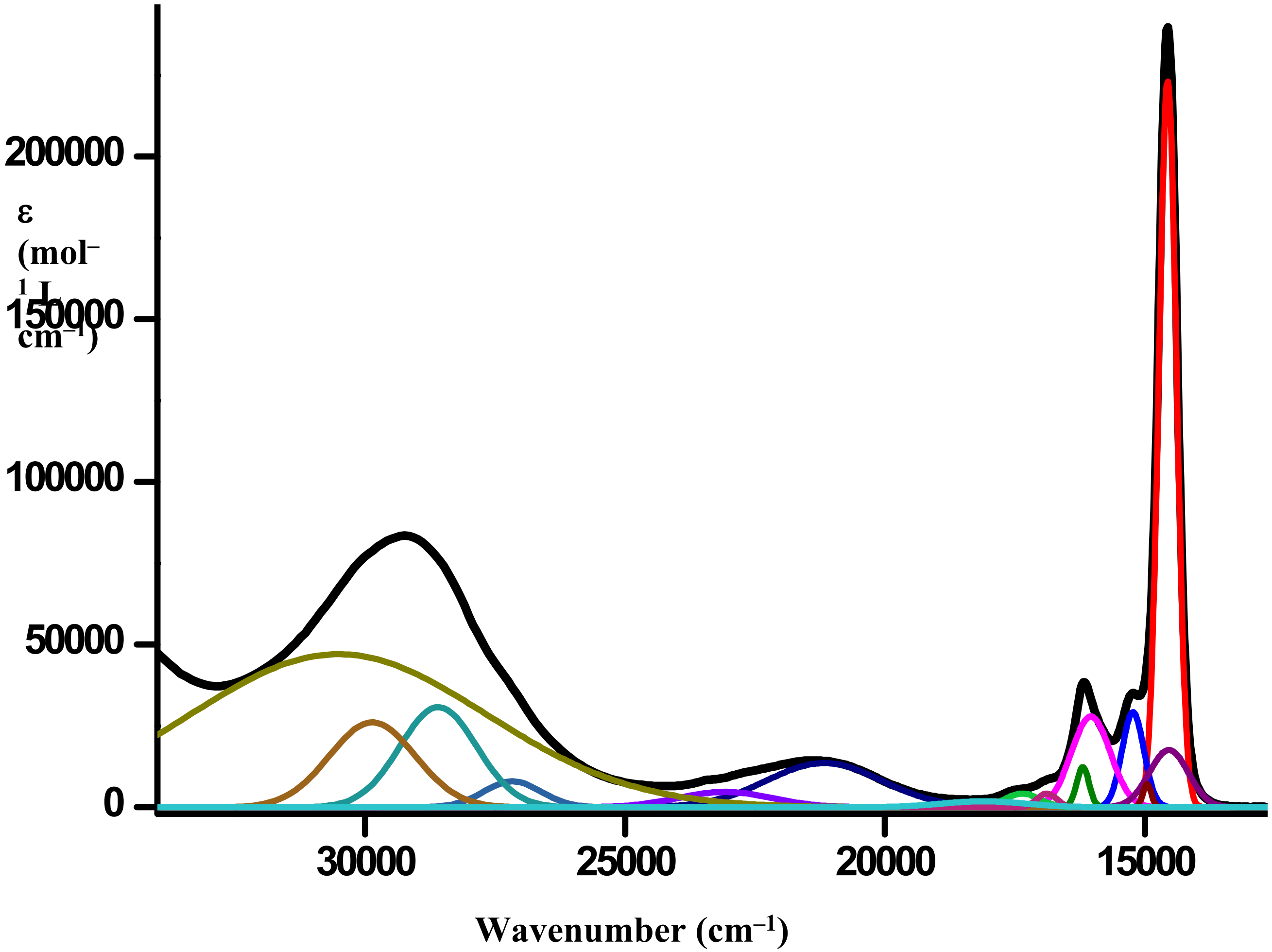

Fig. S22. Solution UV-vis spectrum of the phthalocyaninatoclathrochelate $FeDm_3(B4\text{-}C_6H_4CHO)(HfPc)$ in CH_2Cl_2 (shown in black line) and its deconvolution into the Gaussian components (shown in color lines).

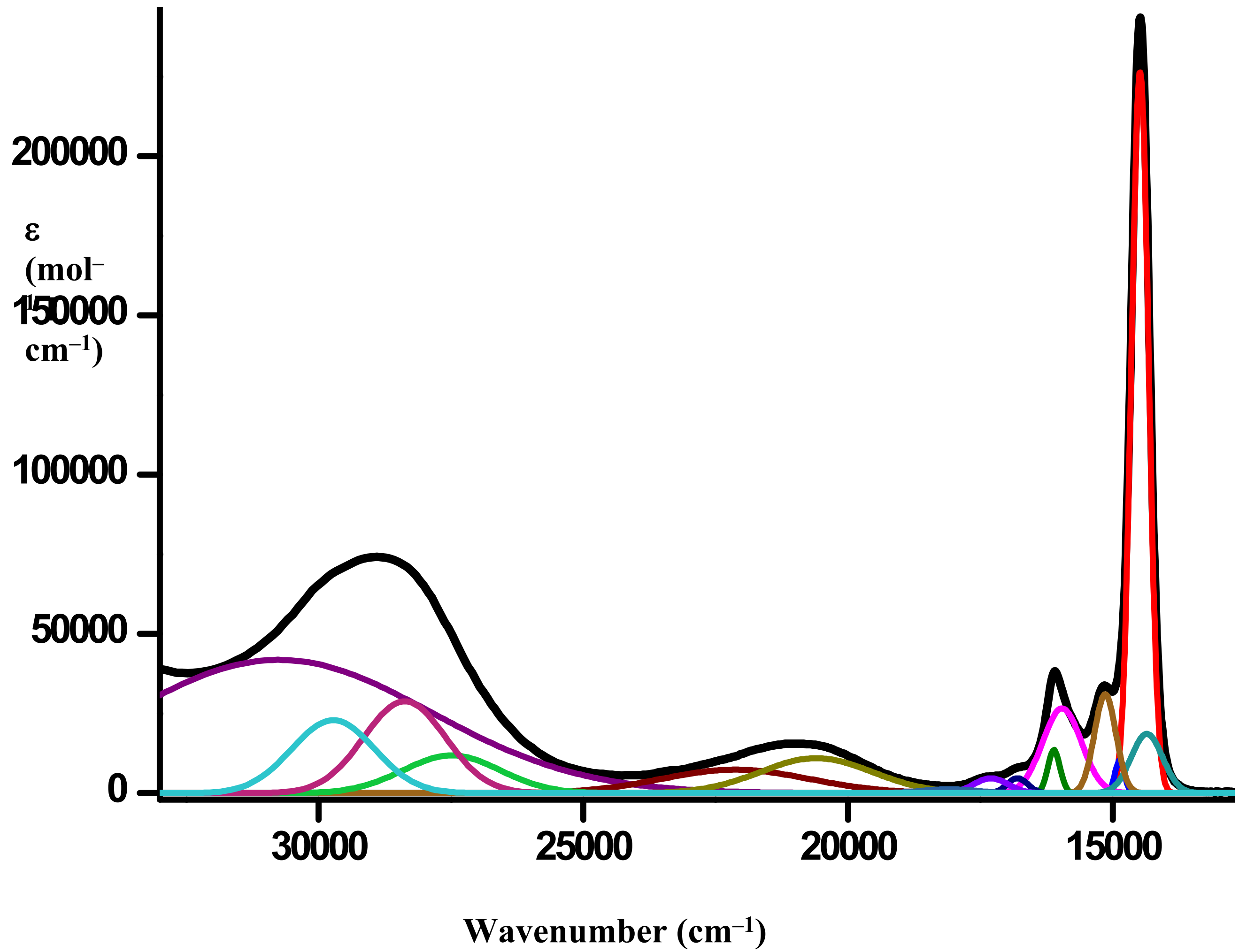

Fig. S23. Solution UV-vis spectrum of the phthalocyaninatoclathrochelate $FeNx_3(B4\text{-}C_6H_4CHO)(ZrPc)$ in 1,2-dichlorobenzene (shown in black line) and its deconvolution into the Gaussian components (shown in color lines).

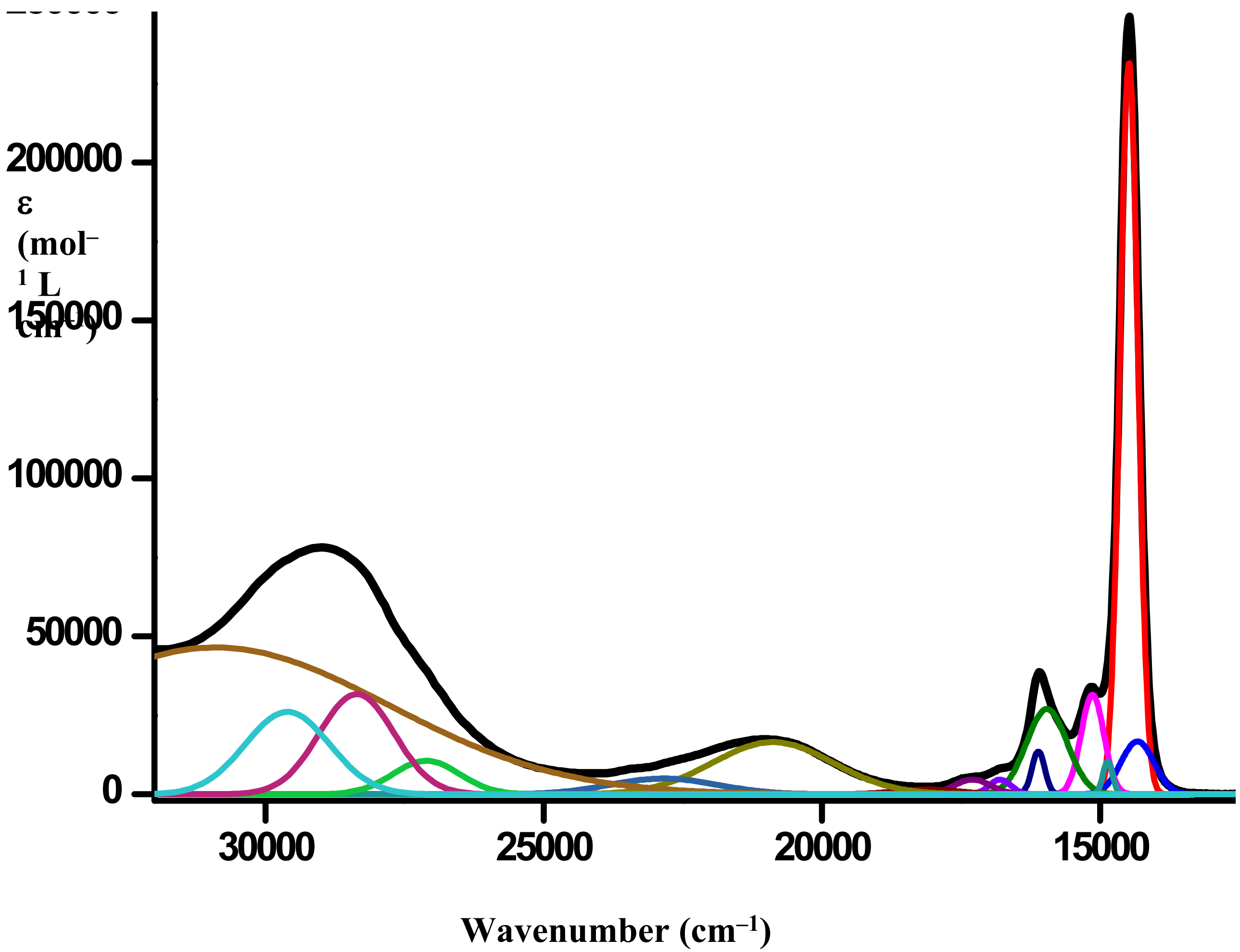

Fig. S24. Solution UV-vis spectrum of the phthalocyaninatoclathrochelate $FeNx_3(B4\text{-}C_6H_4CHO)(HfPc)$ in 1,2-dichlorobenzene (shown in black line) and its deconvolution into the Gaussian components (shown in color lines).

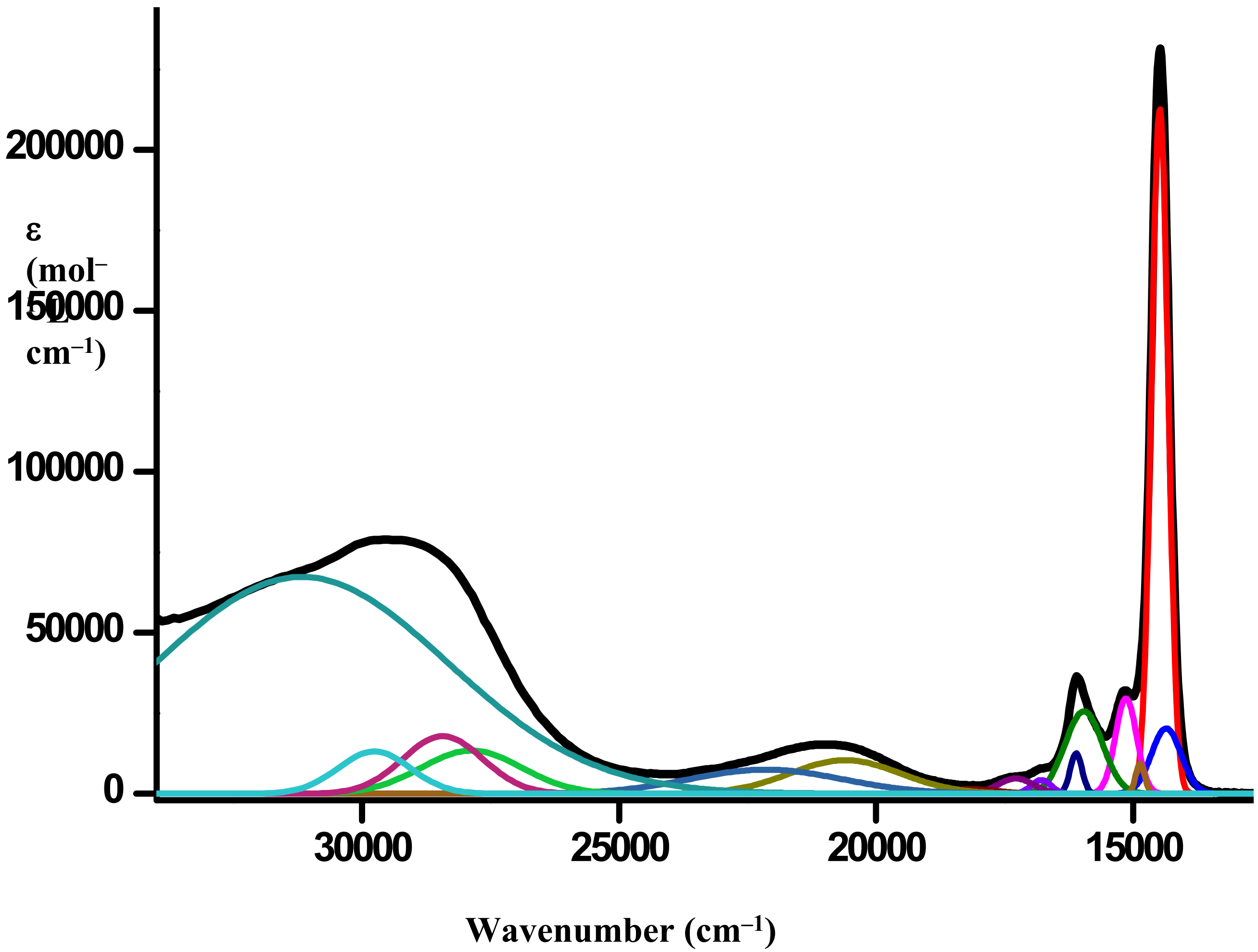

Fig. S25. Solution UV-vis spectrum of the hybrid phthalocyaninatoclathrochelate $FeNx_3(B4\text{-}C_6H_4Id)(ZrPc)$ in 1,2-dichlorobenzene (shown in black line) and its deconvolution into the Gaussian components (shown in color lines).

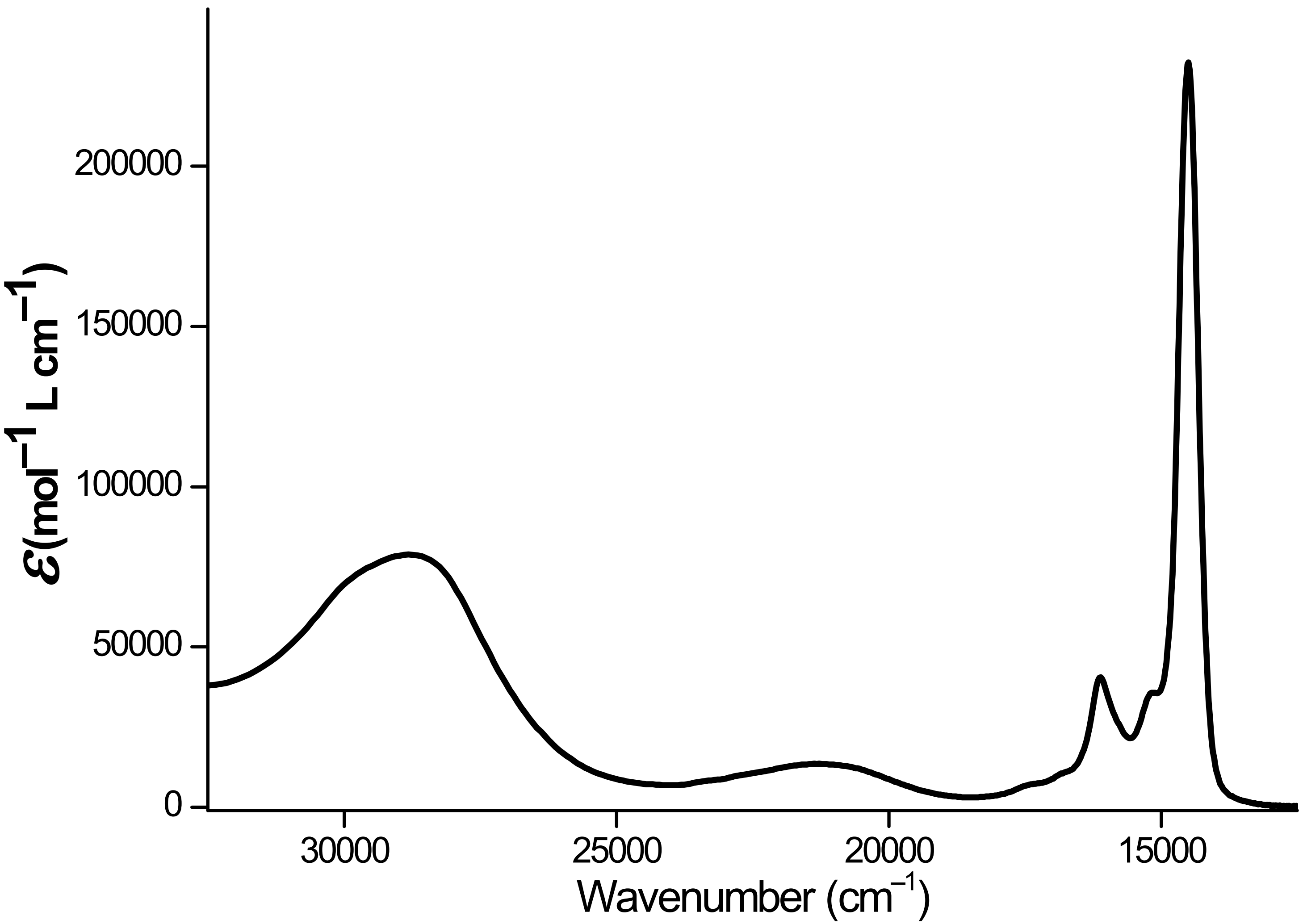

Fig. S26. Solution UV-vis spectrum of the hybrid phthalocyaninatoclathrochelate $FeDm_3(B4\text{-}C_6H_4CHO)(ZrPc)$ in pyridine.

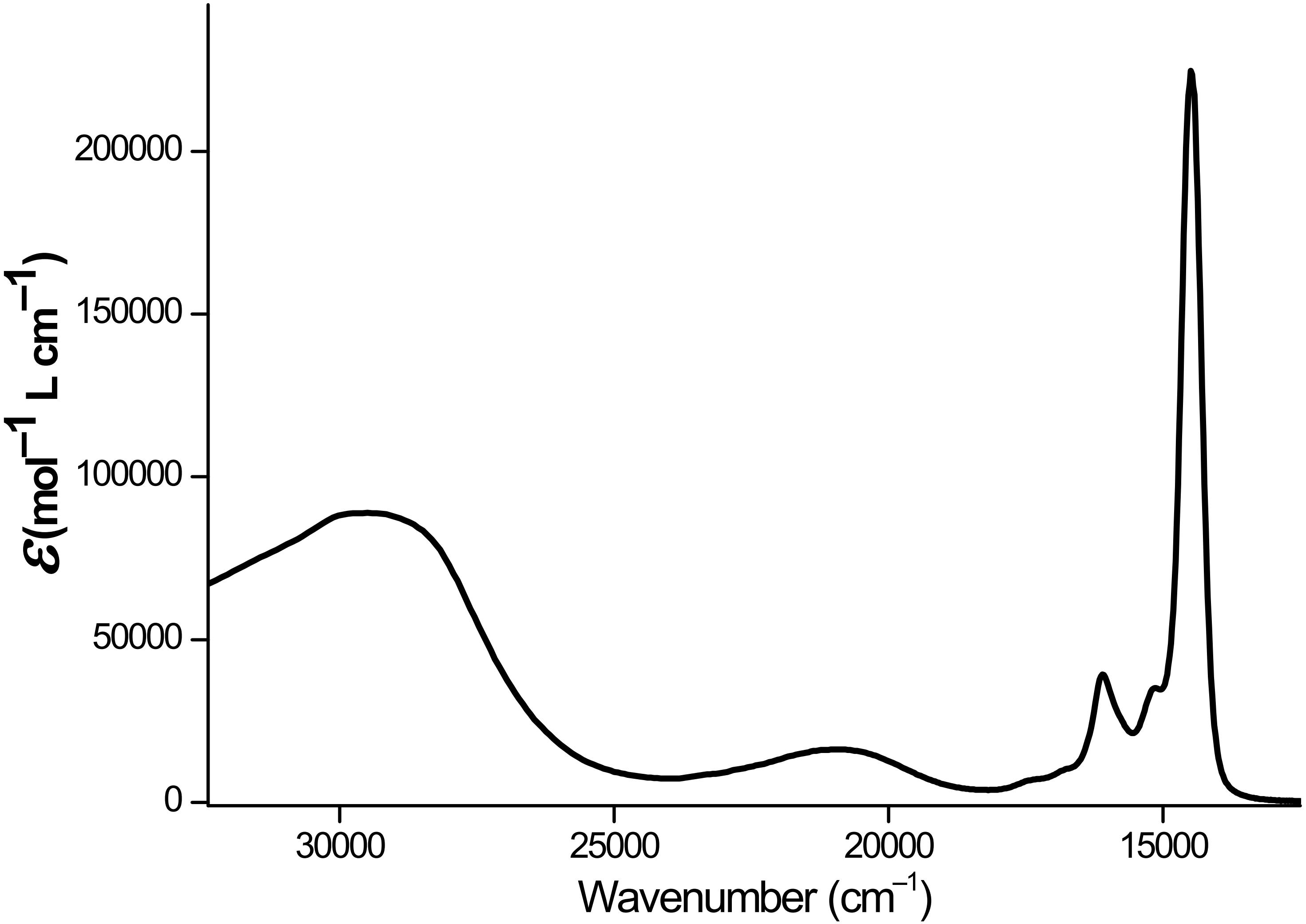

Fig. S27. Solution UV-vis spectrum of the hybrid phthalocyaninatoclathrochelate $FeNx_3(B4\text{-}C_6H_4Id)(ZrPc)$ in pyridine.

Table S1. Solution UV-vis spectra (ν, cm^{-1}, $\varepsilon \times 10^{-3}$, $mol^{-1}Lcm^{-1}$) of the hybrid iron(II) phthalocyaninoclathrochelates under study.

Compound	ν_1	ν_2	ν_3	ν_4	ν_5	ν_6	ν_7	ν_8	ν_9	ν_{10}	ν_{11}	ν_{12}	ν_{13}	ν_{14}	ν_{15}
$FeDm_3(B4\text{-}C_6H_4CHO)(ZrPc)$	14553	14640	14954	15234	16032	16185	16878	17336	18064	20734	22346	27591	28605	29904	30793
	(221)	(19)	(6.2)	(25)	(28)	(13)	(4.0)	(4.2)	(2.3)	(9.1)	(8.2)	(12)	(30)	(26)	(45)
$FeDm_3(B4\text{-}C_6H_4CHO)(HfPc)$	14537	14559	14957	15227	16038	16192	16886	17358	18103	21170	23077	27169	28594	29864	30518
	(18)	(223)	(7.1)	(29)	(28)	(12)	(4.2)	(4.2)	(1.9)	(14)	(4.7)	(8.0)	(31)	(26)	(47)
$FeNx_3(B4\text{-}C_6H_4CHO)(ZrPc)$	14353	14482	14864	15140	15956	16109	16797	17299	18093	20599	22128	27487	28375	29726	30749
	(19)	(227)	(10)	(31)	(27)	(14)	(4.7)	(4.7)	(1.3)	(11)	(7.4)	(12)	(29)	(23)	(42)
$FeNx_3(B4\text{-}C_6H_4CHO)(HfPc)$	14329	14481	14865	15139	15959	16112	16799	17294	18123	20883	22846	27111	28364	29609	30899
	(17)	(232)	(11)	(32)	(27)	(14)	(4.7)	(4.7)	(1.5)	(17)	(5.0)	(11)	(32)	(26)	(47)
$FeNx_3(B4\text{-}C_6H_4Id)(ZrPc)$	14355	14480	14862	15137	15958	16108	16789	17283	18146	20602	22149	27872	28432	29766	31176
	(20)	(213)	(9.4)	(30)	(26)	(13)	(4.2)	(4.8)	(1.4)	(10)	(7.5)	(13)	(18)	(13)	(67)

Table S2. Solution UV-vis spectra (ν, cm^{-1}, ε×10^{-3}, mol^{-1}·l·cm^{-1}) of the (semi)clathrochelate iron(II) complexes

Compound	ν_1	ν_2	ν_3	ν_4	ν_5	ν_6	ν_7
$FeNx_3(B4\text{-}C_6H_4CHO)_2$		22162 (6.8)	23941 (2.8)	31601 (12)	33284 (27)	38309 (12)	
$FeNx(HNx_2)(B4\text{-}C_6H_4CHO)$	19757 (2.0)	21417 (10)	24343 (2.7)	32560 (4.7)	34796 (5.5)	37986 (10)	39823 (24)
$FeDm(HDm_2)(B4\text{-}C_6H_4CHO)$	20306 (4.9)	22168 (6.2)	22986 (3.9)	34516 (1.9)	36214 (6.9)	38144 (4.9)	39251 (20)

Table S3. Crystallographic data and experimental details for the obtained iron(II) phthalocyaninoclathrochelates and their semiclathrochelate precursor

Parameter	FeNx(HNx$_2$)(B4-C_6H_4CHO)	FeNx$_3$(B4-$C_6H_4C(OCH_3)_2$)(HfPc) · 1.5C_6H_6	FeNx$_3$(B4-C_6H_4CHO)(ZrPc) · 3.5$CHCl_3$	FeNx$_3$(B4-C_6H_4Id)(ZrPc)
Empirical formula	$C_{25}H_{31}BFeN_6O_7$	$C_{68}H_{60}BFeHfN_{14}O_8$	$C_{60.5}H_{48.5}BCl_{10.5}FeN_{14}O_7Zr$	$C_{63}H_{50}BFeN_{17}O_7Zr$
Formula weight	594.22	1446.45	1613.74	1315.08
Color, habit	Dark red, plate	Bronze, prism	Red, plate	Violet, prism
Crystal size (mm)	0.53 × 0.47 × 0.08	0.36 × 0.11 × 0.10	0.25 × 0.19 × 0.03	0.16 × 0.14 × 0.09
a (Å)	10.5430(6)	11.8206(2)	13.398(3)	21.989(3)
b (Å)	18.7340(14)	12.7249(3)	15.250(3)	12.810(2)
c (Å)	13.9340(9)	23.8173(5)	17.404(4)	29.843(6)
α (º)	90	101.295(1)	111.16(3)	90
β (°)	109.458(2)	103.735(1)	94.87(3)	103.223(6)
γ (°)	90	95.341(1)	92.81(3)	90
V (Å^3)	2595.0(3)	3375.82(12)	3292.2(13)	8183(2)
Crystal system	Monoclinic	Triclinic	Triclinic	Monoclinic
Space group, Z	P2$_1$/c, 4	P -1, 2	P -1, 2	P 2$_1$/c, 4
D_{cal}(g cm^{-3})	1.521	1.423	1.628	1.067
μ (mm^{-1})	0.639	5.039	1.040	0.356
Reflections collected	36898	53357	45507	100915
Independent reflections (R_{int})	6409 (0.123)	12875 (0.033)	14133 (0.061)	25163 (0.171)
Obs.refl./restraints/ parameters	3280 / 0 / 349	12314 / 24 / 807	11559 / 7 / 878	7442 / 0 / 796
R,^{a} % [F^2> 2σ(F^2)]	0.057	0.044	0.081	0.074
R_w,^{b} % (F^2)	0.132	0.122	0.174	0.116
GOF	1.022	1.117	1.013	0.942
F(000)	1240	1466	1630	2696

$^aR = \Sigma||F_o|-|F_c||/\Sigma|F_o|$. $^bR_w = [\Sigma(w(F_o^2-F_c^2)^2)/\Sigma(w(F_o^2))]^{1/2}$. $^c\mathrm{GOF} = [\Sigma w(F_o^2-F_c^2)^2/(N_{obs}-N_{param})]^{1/2}$